ADDIS ABABA UNIVERSITY

ADDIS ABABA INSTITUTE OF TECHNOLOGY

SCHOOL OF MECHANICAL AND INDUSTRIAL ENGINEERING

Analytical and Finite Element Analysis of Surface Wear on Disc Brake Rotor

A Thesis

Submitted to

The School of Mechanical and Industrial Engineering

For Partial Fulfilment

of the Requirements for the Degree of

Master of Science in Mechanical Engineering (Mechanical Design)

By

Hailemariam Shegaw Abebaw

Advisor: Dr. Daniel Tilahun

April/2015

Addis Ababa, Ethiopia

Declaration

I, the undersigned, declare that this thesis is my original work and has not been presented for any degree in any university and all the sources of materials used for the thesis have been fully acknowledged.

Hailemariam Shegaw Abebaw

Name Signature

Place: Addis Ababa Institute of Technology, Addis Ababa University, Addis Ababa, Ethiopia

Date of Submission: 24/04/2015

Approved by board of examiners

Dr. Daniel Tilahun		08/05/15
Dean ~~Head~~ of the school	signature	date
Dr. Daniel Tilahun		08/05/15
Advisor	signature	date
Tolosa Deberie		11/05/15
Internal examiner	signature	date
Dr. Tamrat Tesfaye		11/05/15
External examiner	signature	date

Director of Postgraduate Program
Addis Ababa University
Addis Ababa Institute of Technology

Abstract

A particular type of dry contact condition, known as disc and pad brake in contact, in which exposed to wear. In this thesis the wear analysis of disc brake is analyzed by using analytical and finite element method during short brake condition. One particular existing disc brake design for a SUV car of model DD6470C is selected for the study. The dimensions, material property and maximum allowable speed and variable applied brake pressure of this car are used as an input both for analytical and finite element method. Analytical analysis of distribution of contact temperature along in radial direction of disc brake caused by applied heat flux is solved by using separation of variable method. Finite element model of disc and pad brake assembly is done using the CATIA software. Finite element simulation for contact pressure and von misses stress using ANSYS workbench for the case of the structural analysis of disc brake is done by applying only brake pressure and angular velocity. But, in the case of thermal-structural analysis the maximum contact temperature value of disc and pad is considered in addition to applied brake pressure. The contact pressure and von misses stress are calculated analytically and ANSYS workbench results are presented in contour plot and numerically. Contact pressure, von misses stress and wear depth are increasing as increasing of both brake pressure and contact temperature of disc in case of thermal-structural analysis. The structural analysis is less effect than that of thermal-structural analysis in all contact pressure, von misses stress and wear. Based upon the analytical and ANSYS workbench analysis, an analytical model of dry sliding wear was developed. A multi-aspect comparison between analytical and ANSYS workbench results were made. A good agreement between analytical and ANSYS workbench results shows that model provided a reliable prediction of the tribological systems of disc-pad contact. The critical point of contact for disc in contact with pad in the case of structural analysis is near to inner and outer radius of disc brake while thermal-structural is at 95.859mm along radial direction from its center. Thus, this study provides effective reference for design and engineering application of brake disc and brake pad.

Key words: Analytical analysis, finite element method, contact pressure, wear

Acknowledgments

I would like to express my appreciation to my supervisor, Dr.Daniel Tilahun for his unbounded encouragement, guidance, support and help during my thesis paper. It has no doubt that it is his attentiveness and professional experience inspiring me to go to the end of it with confidence.

I also would like to give my thanks to my friends Mr. Esayas Lateno and Mr. Shiferaw Damtie for their help and discussion on finite element method. The thanks also extend to my brother Challachew Setegn provided a room to me and for his help during my thesis paper.

Thanks are also delivered to Mr. Aby Abebe give me continuous help and advice to fulfill the paper. The gratitude is also extended to all the other friends giving help, encouragement and concerns to me during my thesis study.

Finally, I would like to give my appreciation to my parent their support, encouragement, understanding and love as always.

Table of Contents

List of Figures

List of Tables

Nomenclature

K	dimensionless wear coefficient
P	contact pressure and
H	hardness of the soft material
V	sliding speed
h	height loss per unit time
δ	disc thickness
ρ	density
k	thermal conductivity
c	specific heat
ν	poisson's ratio
α	thermal expansion
E	elastic modulus,
μ	coefficient of friction
P_d	brake pressure
ϕo	cover angle of pad in degrees
r, z, θ	radial circumferential and axial coordinate
Γ	contact surface area between pads and disc (upper)
h_4	convective heat transfer surface area of pad
h_3	convective heat transfer surface area at external radius of disc brake
h_2	convective heat transfer surface area at internal radius of disc brake
h_1	surface area of disc exposed to convective heat transfer
h_5	convective heat transfer surface area at vents
h_6	adiabatic surface area at half of disc brake thickness

δ_p	thickness of pad
δ_d	thickness of disc
δ_t	thickness of vent
p	applied force
r_o	external radius of disc brake
r_i	internal radius of disc brake
$\sigma_{zz}(r)$	longitudinal stress as function of radial distance
$\sigma_{rz}(r)$	shear stress as function of radial distance
$q(r,t)$	heat flux as function of radial distance and time
$v(t)$	velocity of car with respect to time
$p(r)$	contact pressure along radial direction
r	radial distance
t	time
μ	coefficient of friction between the brake pad and rotor
$\frac{\partial T}{\partial z}$	partial derivative of contact temperature with respect to z-direction
$\frac{\partial T}{\partial r}$	partial derivative of contact temperature with respect to r-direction
k_d	thermal conductivity of disc brake
$T(r,z,t)$	temperature distribution with respective to r, z-direction and time
q_{do}	heat flux of disc brake at time zero
T_∞	ambient temperature
T_0	initial temperature of disc brake
t_s	stopping time during brake
k_p	thermal conductivity of pad brake

F	applied force
a	contact radius of flat ended punch
p(x)	contact pressure along in axial direction
P_b	applied hydraulic pressure
Ac	surface area of the pad in contact with the disc and
$F_{friction}$	frictional force generated by the brake pads
F_{clamp}	clamp force generated by the caliper
ϑ	index in contact pressure for analytical analysis
v_d	poisson's ratio of disc brake
v_p	poisson's ratio of disc brake
G_d	shear modulus of materials disc
G_p	shear modulus of materials pad
E_d	modulus of elasticity of disc brake
E_p	modulus of elasticity of pad brake
P_c	contact pressure for analytical analysis structural analysis
k	dimensional wear coefficient (mm^2N/m)
h_s	wear depth (mm) by effect brake pressure
s	sliding distance
R_m	mean radius of internal and external radius of disc brake
p_o	contact pressure at $r = 90mm$
ω_o	angular velocity of disc brake at time equal to zero
ρ_d	density of disc brake
c_d	specific heat of disc brake
k_d	thermal conductivity of disc brake

ρ_p	density of pad brake
c_p	specific heat of pad brake
k_p	thermal conductivity of pad brake
K_d	thermal diffusivity of disc brake
N_u	Nusselt number, d'less
C	heat transfer coefficient, d'less
R_e	Reynolds number, d'less
pr	Prandtl number, d'less
c_a	specific heat of air
h_R	convective heat transfer coefficient
k_a	thermal conductivity of air
m	heat transfer parameter, d'less
n_h	heat transfer parameter, d'less
ρ_a	density of air
μ_a	viscosity of air
L_c	characteristic length of vane or length of cooling vane
h_R	heat coefficient inside the vanes of the brake rotor
d_h	hydraulic diameter
$V_{average}$	average velocity in vane
V_{out}	outlet velocity of the cooling vanes
V_{in}	inlet velocity of the cooling vanes
A_{in}	inlet area of vane
A_{out}	outlet area of vane
D	outer diameter of the rotor

d	inner diameter of the rotor
n_r	revolutions per minute of rotor
R_e	Reynolds number
$\theta(r,z,t)$	dimensionless temprerature
Z	dimensionless distance from the center along z-direction
R	dimensionless radial position
W	dimensionless radial position
Bi	Biot-number
τ	Fourier number
λ	equating constant for dimensionless heat with respect dimensionless time
ξ	equating constant for dimensionless heat with respect dimensionless Z direction
ς	equating constant for dimensionless heat with respect dimensionless R-direction
φ	represent the indicial root
$C_1, C_2, \ldots, C_5$	constant of integrations
$H_1, \ldots, H_4$	constant of integrations
K_1, K_2	summation of series
$T_c(r)$	contact temperature distribution for disc brake
P_t	contact pressure with the effect of brake pressure and temperature
a_t	contact radius of temperature effect
Pe	Peclet number
h_t	wear depth by the effect of both temperature and pressure
σ_e	von mises stress

σ_1, σ_2 and σ_3	principal stress
s_y	yield strength
n	factor of safety
σ_{zz}	stress normal direction
σ_{zrS}	stress shear direction
σ_{zrT}	stress torsion direction
σ_{es}	von misses analysis by structural effect
σ_{et}	von misses stress analysis for thermal and structural effects
σ_r	radial stress
σ_θ	tangential stress
σ_z	normal stress
c_p	constraint pressure
K_t	stress concentration factor
σ_{max}	actual maximum stress
σ_o	normal stress

Chapter One

1. Introduction

1.1. Background of the Study

A brake is a device by means of which artificial frictional resistance is applied to moving machine member, in order to stop the motion of a machine. Modern cars have disc brakes on the front wheels, and there is a growing trend to have them on the rear wheels as well. The braking process is in fact the matter of energy balance and aim of braking system is to transform mechanical energy of moving vehicle into some other form, which results in decreasing the speed of the vehicle. The kinetic energy is transformed into the thermal energy by means of dry friction effects, which then is, dissipated into the surroundings [1]. A brake disc rotor is firmly fitted to and rotates with the wheel. Two brake pads are positioned inside a caliper mounted on the knuckle, which is mounted on the chassis. When the driver hits the brakes, the brake cylinder pressure increases and the piston pushes the pads into contact with the disc. The friction force between the brake pads and disc exerts braking torque on the disc, which is connected to the wheel, and the subsequent friction between the tire and the road makes the car slow down. An example of a disc brake assembly that consists of a ventilated disc, a cross-section of a sliding caliper with a single piston, and two brake pads is presented in Figure 1.1.

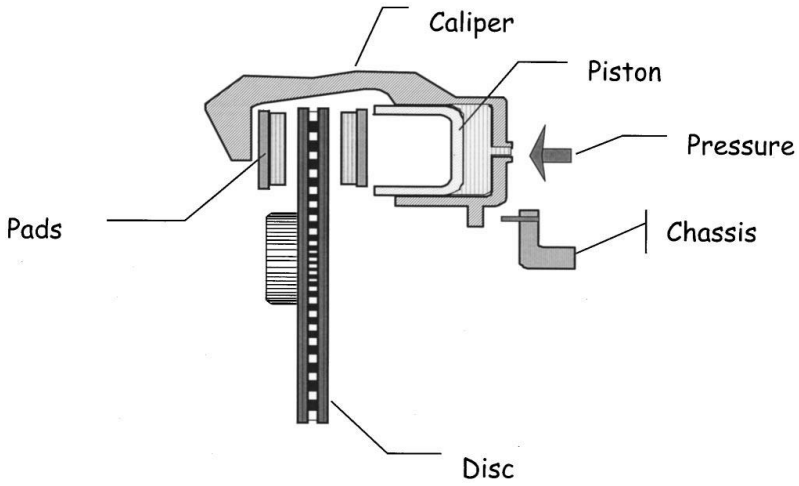

Figure 1.1: Disc and pad brake assembly with a single-piston and a ventilated disc [2]

An interaction between a brake disc and pads of automotive brake is characterized by a number of dry contact phenomena. These phenomena are influenced by brake operation conditions (applied pressure, speed, and brake interface temperature) and material

characteristics of a friction couple. The coefficient of friction should be relatively high and keep a stable level irrespective of temperature change, humidity, age, degree of wear and corrosion, presence of dirt and water spraying from the road [3]. During braking surface temperature generated in contact areas has a major influence on wear, scuffing, material properties and material degradation. Due to these reasons, this thesis focuses on surface wear analysis of disc brake. Wear , according to Bayer, is defined as "damage to a surface as a result of relative motion with respect to another substance" [4]. For the purposes of this work, wear shall be defined as the loss of material from a surface due to sliding along another surface. Two methods of classifying wear are: (1) the conditions in which the wear occurs; and (2) the mechanism by which the wear occurs [4]. Conditions used to classify wear include whether or not there is a lubricant present, and whether or not there are hard, abrasive particles present. If there is a lubricant present, it is referred to as lubricated wear , otherwise it is dry wear [5]. If there are abrasive particles causing wear , then it is referred to as abrasive wear , otherwise it is called sliding wear [5].The current study focuses on dry sliding wear. So in order to analysis this type of wear, We have chosen to use the conventional and well-established ARCHARD'S law of wear [6], which gives the wear rate h (height loss per unit time) through the relation.

$$h = \frac{KpV}{H} \quad \text{..... (1.1)}$$

Where

K is the dimensionless wear coefficient

p is the contact pressure

H is the hardness of the soft material

V is the sliding speed

h is the height loss per unit time

1.2. Statement of the Problem

The overall parts of automotive, besides engines, there are more crucial parts that engineers need to look into consideration. Suspension, brake, electrical, hydraulic and gear are all the crucial systems in the automotive areas. Each of all system has their own functionality which brings life to the automation industries. Brakes is such a crucial system in stopping the vehicle on all moving stages including braking during high speed, sharp cornering, traffic jam , downhill and repeated braking. All of those braking moments give a different value of contact pressure distribution, contact temperature distribution, thermal stress, contact pressure distribution due to temperature and applied pressure effect, frictional heat generate during braking and wear out of parts. Due to this, many researches are done on pad and disc brake rotor but their main concern is the contact pressure, thermal stress analysis, temperature distribution, wear using finite element analysis for contact pressure, temperature distribution and fatigue analysis. Wear has been recognized as meaning the phenomenon of material removal from a surface due to interaction with a mating surface. Almost all machines lose their durability and reliability due to wear and the possibilities of new advanced machines are reduced because of wear problems. Therefore, study for wear analysis has become a strong need for this thesis work. In this thesis both finite element analysis using ANSYS work bench software and analytical formulation of wear are used for disc brake rotor, and finally comparing the results obtained. The purpose of study wear of disc brake rotor is to increase the life of it and efficiency of the brake.

1.3. Objective of the Study

1.3.1. Main Objective

The main objective of this thesis paper is to analyze surface wear on disc brake rotor analytically and numerically.

1.3.2. Specific Objectives

- To identifying contacts points in which, disc –pad brake contact, exposed worn out on both structural and thermal-structural effects.
- Modeling of pad and disc brake rotor system to study contact using finite element analysis software to study the contact pressure analysis and comparing results with analytical formulation.
- To estimate of von misses stress in the contact condition between pad and disc brake rotor by finite element software and analytical analysis.
- To estimate contact pressure for disc and pad in contact in both structural and thermal-structural effects.
- Obtain analytical solutions for transient two- dimensional conduction problem in ventilated disc brake and pad using the method of separation of variables.
- Solve the transient conduction problem in ventilated disc brake and pad , and predict the variation of temperature with time and along radial direction.
- Estimate wears depth in short brake condition by using ARCHARD equations.

1.4. Methodology of the Study

Begin with a literature review, a lot of paper and journal have been read up and a part of it has been consider in this thesis work. Meanwhile, the mechanical and thermal properties and geometric parameters of this studied component are shown in tables. The source of the data for disc and pad are taken from previous thesis [7]. Later, the two-dimensional and three-dimensional drawings of disc and pad assembly have been done by using Auto-cad and CATIA V5R16 respectively. The analytical contact pressure distribution is model based on combination of hertz and non-hertz contact theory to obtain an approximate estimate of contact pressure distribution caused applied brake pressure for structural analysis. The contact temperatures of disc and pad brakes are solved from partial differential heat equation by using separation of variable method. Then after, we are used Tian and Kennedy formula in which relates contact temperature of disc brake to relate with contact pressure of it. Contact pressure distribution estimate by using ANSYS workbench for structural and thermal-structural analysis. Structural analysis is done by applied brake pressure and angular velocity of disc brake. But, thermal-structural analysis are done by applied brake pressure, both contact temperatures of disc and pad. We use these contact pressures results solved by analytical method and ANSYS workbench for structural and thermal-structural analysis to predict the wear thickness of disc brake under ARCHARD wear model is used.

1.5. Organization of the Thesis

This thesis is organized in to six chapters. In the first chapter, background and justification of thesis work and the objectives to be achieved are discussed. In chapter two, a review of literature relevant to this thesis work, which has been investigated by different researchers, is given. Analytical methods and conditions are discussed in chapter three. The discussion is started with material properties, different assumption and conditions of the study. These is followed by contact pressure distribution and wear analysis for structural analysis, contact surface temperature, contact pressure distribution and wear analysis for thermal-structural analysis. Finally, von misses stress analysis for structural and thermal- structural analysis is also discussed. Next, in chapter four finite element methods and conditions are discussed. Three dimensional finite element analysis is done by ANSYS workbench. Also different static structural and thermal-structural boundary and conditions are discussed in detail. Furthermore application of symmetric boundary condition is indicated here. In chapter five results of the analysis are summarized and discussions are made based on the outputs of the finite element method. In addition, comparison of analytical and numerical solutions is made. Finally, chapter six gives conclusion achieved from this thesis work and propose future work in this field of study.

Chapter Two

2. Literature Review

Wear can take place when two or more bodies in frictional contact slide against each other. The significant effect of it, particularly in friction material of disc brake system, is reduction of its life span. Taking this to consideration, many researchers have done about the disc brake related to wear analysis.

Talati, Faramarz (2009), presented a paper on analysis of heat conduction in a disk brake system. In their paper, the governing heat equations for the disk and the pad are extracted in the form of transient heat equations with heat generation that is dependant to time and space. In the derivation of the heat equations, parameters such as the duration of braking, vehicle velocity, geometries and the dimensions of the brake components, materials of the disk brake rotor and the pad and contact pressure distribution have been taken into account. The problem is solved analytically using Green's function approach. It is concluded that the heat generated due to friction between the disk and the pad should be ideally dissipated to the environment to avoid decreasing the friction coefficient between the disk and the pad and to avoid the temperature rise of various brake components and brake fluid vaporization due to excessive heating.

Belchocine, Ali (2012), presented paper on thermal analysis of a solid brake disc. The objective of their study is to analyze the thermal behavior of the full and ventilated brake discs of the vehicles using computing code ANSYS. In their analysis approach is to create the model CFD which contains the fields to be studied in ANSYS Workbench. Three different grade of cast iron is chosen (FG 25 AL, FG20, and FG15). The numerical simulation shows that radial ventilation plays a very significant role in cooling of the disc in the braking phase. The variation in temperature between a full and ventilated disc having same material is about 60 degree at the moment1.8839 s from application of brake. The obtained results are very useful for the study of the thermo mechanical behavior of the disc brake (stress, deformations, efficiency and wear).

Harpal, Singh (2012), presented paper on thermal analysis of disc brake using comsol, in this paper Finite element analysis techniques is used to predict the temperature distribution and identify the critical temperature of brake disc. Considering all three modes of heat transfer (conduction, convection and radiation) for three different materials of rotor disc are

been used (cast iron, aluminum and ceramics). It is concluded that cast iron can be used in brake disc which will give moderate cooling at low temperature as compared to other. Ceramics has good cooling characteristics but it is costly, can be used in racing cars where high temperature is produced.

Sowjanya, K. (2013), presented paper on structural analysis of disk brake rotor. Disc brake is usually made of Cast-iron, so it is being selected for investigating the effect of strength variations on the predicted stress distributions. Aluminum Metal Matrix Composite materials are selected and analyzed. The domain is considered as axis-symmetric, inertia and body force effects are negligible during the analysis. The model of Disc brake is developed by using Solid modeling software Pro/E (Cero-Parametric 1.0).Further Static Analysis is done by using ANSYS Workbench. Thermal solution to the structural analysis and the maximum Von Misses stress was observed to be 50.334 M Pa for CI, 211.98 M Pa for AlMMC1, and 566.7 M Pa for AlMMC2, the Brake disc design is safe based on the Strength and Rigidity Criteria.

Kuo, G.C. (2009), presented paper on transient temperature analysis of a cylindrical heat equation. The method of superposition and separation variables is applied to gain analytical solutions to the transient heat conduction for a two dimensional cylindrical fin. The temperature distributions are generalized for a linear combination of the product of Bessel function, Fourier series and exponential type for nine different cases. The solutions presented in this study can be used to verify the two- or three-dimensional numerical conduction codes. Relevant connections with some other closely-related recent works are also indicated.

Shah, Q.H. (2011), presented paper on surface temperature distribution in a composite brake rotor. The prediction of surface temperature for brake rotor is regarded as an important step in studying the brake system performance. The frictional heat generated on the rotor surface can influence excessive temperature rise which in turn leads to undesirable effects such as thermal elastic instability, premature wear, brake fluid vaporization and thermally excited vibrations. The purpose of this study is to investigate the temperature distribution profile for brake caliper pressure application of 0.5, 1.0, 1.5 and 2.0 MPa with a speed of 60km/h braking condition on the disc rotor surface. The brake rotor assembly is built by using a three- dimensional finite element model of a real car brake rotor. To verify the simulation results, an experimental investigation is carried out. It is believed from the study that composite brake rotor influences the temperature distribution and heat dissipation rate which could prevent excessive temperature rise and subsequently prolong the service life of the

rotor. The finite element method is cost effective and also assists the automotive industry in producing optimized and effective brake rotor for thermal distribution analysis.

Belhocine, Ali (2014), presented paper on structural and contact analysis of disc brake assembly during single stop brake event. An automobile disc brake system is used to perform three basic functions, i.e. to reduce speed of a vehicle, to maintain its speed when travelling downhill and to completely stop the vehicle. During these braking events, the disc brake may suffer of structural and wear issues. It is quite sometimes that the disc brake components fail structurally and/or having severe wear on the pad. Thus, his paper aims to examine stress concentration, structural deformation and contact pressure of brake disc and pads during single braking stop event by employing commercial finite element software, ANSYS. The paper also highlights the effects of using a fixed caliper, different friction coefficients and different speeds of the disc on the stress concentration, structural deformation and contact pressure of brake disc and pads, respectively. Results from the investigation could provide a better explanation of the variation in contact pressure distribution and in turn squeal generation. Thus, his study provides effective reference for design and engineering application of brake disc and brake pad.

Tirovic, M. and G. Ali (2001), friction brakes are exposed to high mechanical and thermal loads. Mechanical loads are generated by clamping, friction and centrifugal forces, as well as by brake acceleration in different directions whereby the thermal loads are the result of the frictional heat generation on the brake friction surfaces. They also stated that thermal loads are often much more severe than mechanical loads and also much more difficult to predict accurately. As a result, the design process for most brake concepts is concentrated on thermal loads.

Imam, Syafa'at (2012), presented paper on Prediction of Sliding Wear of Artificial Rough Surface. When two surfaces are brought in contact, deformation takes place at asperity level. The local pressure distribution and deformation of the contacting surface are importance with respect to wear. This paper describes a wear model to predict the wear of rough sliding contacts. The wear model is based on the general Archard's wear equation in combination with finite element analysis (FEA). In this paper the roughness is represented by uniformly distributed spherical asperities. The proposed model, FE in combination with Archard's wear law, has proven to be a powerful tool in predicting wear of rough surfaces.

Alen, John (2014), presented paper on Stress Analysis of Polyoxymethylene which Leads to Wear in Pin on Disc Configuration using Finite Element Method. The wear is defined as the progressive loss of substances from the operating surface of a body occurring as a result of relative motion at the surface. The simulation of the stresses which leads to wear in pin on disc configuration having the pin made of polyoxymethylene having the NC010-150 designation in sliding contact with the rotating steel disc was performed using finite element software ANSYS Workbench11.0. The three dimensional geometry of the required configuration was made by using the modeling software CATIA. Using the boundary conditions the analysis were done. Rotation of 3000 rpm was provided for the disc. Then with analysis software he was analyzing the wear by varying the pressure acted up to the tensile yield strength of the material and assuming that the region of the pin where maximum equivalent stress occurred is failing or wearing out, since he had no provision for finding out the wear analysis in the available software packages. Then he was removing the failed elements and again repeating the same process until the material of the pin fails completely, i.e. varying the length of the pin. Along with that the maximum deformation and the maximum equivalent stresses are noted. Then compare the results of deformation and the equivalent stress and concluded that when the length of the pin decreases (pin failed more) the deformation is decreasing and the equivalent stress is increasing. When the load exceeds tensile yield strength of the material then the material is failed under these circumstances.

Molinari, J.F. (2000), presented paper concerned with the calibration and validation of a finite-element model of dry sliding wear in metals. The model is formulated within a Lagrangian framework capable of accounting for large plastic deformations and history-dependent material behavior. He resort to continuous adaptive meshing as a means of eliminating deformation-induced element distortion, and of resolving fine features of the wear process such as contact boundary layers. Particular attention is devoted to a generalization of ARCHARD'S law in which the hardness of the soft material is allowed to be a function of temperature. This dependence of hardness on temperature provides a means of capturing the observed experimental transition between severe wear rates at low speeds to mild wear rates at high speeds. Other features of the numerical model include: surface evolution due to wear; finite-deformation, thermo plasticity; heat generation and diffusion in the bulk; non-equilibrium heat-transfer across the contact interface; and frictional contact. The model is validated against a conventional test configuration consisting of a brass pin rubbing against a rotating steel plate.

Podra, P., Andersson, S. (1999), had studied the wear simulation approach with commercial finite element software ANSYS. A modeling and simulation procedure was proposed and used with the linear wear law and the Euler integration scheme. A spherical pin on-disc unlubricated steel contact was analyzed both and the Lim and Ashby wear map was used to identify the wear mechanism. It was shown that the FEA wear simulation results of a given geometry and loading can be treated on the basis of wear coefficient-sliding distance change equivalence. The finite element software ANSYS was well suited for the solving of contact problems as well as the wear simulation. The actual scatter of the wear coefficient was within the limits of 40-60% led to considerable deviation of wear simulation results. Due to the model simplifications and the real deviation of input data, the FEA wear simulation results was evaluated on a relative scale to compare different design options, rather than to be used to predict the absolute wear life.

Chapter Three

3. Analytical Methods and Conditions

3.1. Gray Cast Iron Material Composition and Thermo-Elastic Properties

A disk brake rotor is generally made from gray cast iron due to cast iron provides good wear resistance with high thermal conductivity, high thermal diffusivity, and low production cost compared to other disc brake rotor materials such as AL-MMC, carbon composites and ceramic based composites [20]. Due to this reason it is a material that has been commonly used to create components of varying complexity for a long time. Gray cast iron's high damping capacity, combined with its excellent machinability and high hardness, is unique to this material and makes it ideally suited for machine bases and supports, engine cylinder blocks and brake components (Table 3.1).

Table 3.1 Gray Cast Iron Specifications, Characteristics & Applications

Standard Specifications	Characteristics	Applications
ASTM A48: gray iron castings ASTM A74: cast iron soil & pipe fittings ASTM A126: gray iron castings for valves, flanges & pipe fittings ASTM A159: automotive gray iron castings SAE J431: automotive gray iron castings	Several strength grades; Low rate of thermal expansion Resistance to thermal fatigue; Lubrication retention; and good machinability.	Automobile engine blocks & heads, clutch; Internal combustion engines machine tool bases; Brake components

The properties of gray iron are primarily dependent on its composition. Normally, cast iron consists of two main substances: graphite (carbon) flakes and matrix ferrous metal. Both of these constituents have a significant influence on the stress-strain response of the material. This is because of the weak bonding between the graphite flakes and metal matrix which causing gaps or voids to open in the material under tension. Therefore, the compressive

strength of cast iron is two or three times higher than its tensile strength, even though isotropic material property is used in this thesis [21]. In order to capitalize on this condition, the cast iron product should be designed to be loaded in compression wherever possible. The presence of the graphite provides several valuable characteristics to cast iron. These include:

- The ability to produce sound castings economically in complex shapes such as water cooled engine blocks
- Dimensional stability under differential heating such as in brake drums and disks.
- High vibration damping as in power transmission cases, and brakes.
- Border line lubrication retention as in internal combustion engine cylinders.

Iron accounts for more than 95%, while the main alloying elements are carbon and silicon. Cast irons contain appreciable amounts of silicon, and consequently these alloys should be considered ternary Fe-C-Si alloys. Appreciable silicon content is necessary in gray iron because this element causes the precipitation of the graphite in the iron. Silicon also imparts corrosion and elevated temperature oxidization resistance to gray iron. Here graphite is present in the form of flakes.

To classify gray iron in accordance to its thermo elastic properties, ASTM (American Standard of Testing Material) Standard A48 and SAE (society of Automotive Engineer) Standard J431 provide the best details to accomplish this task. The two specifications approach the task from different standpoints but essentially the concept remains the same. For example, the number in a Class 30 gray iron refers to the minimum tensile strength in ksi. In SAE Standard J431, a minimum tensile strength to hardness ratio is required. The class then is identified as a grade. Class 30A indicates that the iron must have a 30 ksi (207 MPa) tensile strength in an "A" bar (0.875in. as cast diameter). In SAE Standard J431, tensile strength is not required, but hardness and a minimum tensile strength to hardness ratio are required. The class then is identified as a grade. Properties of gray cast iron materials were adopted from the previous study of Belhocine and Bouchetara [21] which are related to SAE or ASTM specification (Table 3.2 and Table 3.3).

Table 3.2 Mechanical Properties of the Disc and Pad

Material Properties	Density, ρ (kg/ m3)	Poisson's Ratio, v	Tensile Strength, σy(MPa	Modulus of Elasticity, E (GPa)	Compression to tensile Ratio	Brinell Hardness (MPa)
Disc	7250	0.28	350	130	3.84	220
Pad	1400	0.25	350	130	3.84	220

Coefficient of friction between pad and disc brake rotor 0.35 is taken from previous study [7]. For normal car and light truck applications, the SAE specification is J431 G3000 (ASTM Class 30). This specification dictates the correct range of hardness, chemical composition (Carbon 3.20-3.50%, Silicon 1.90-2.30%, Manganese 0.60-0.90%, Sulfur (0.02-0.25%), Phosphorus (0.02-1%)), tensile strength, and other properties necessary for the intended use. There are no generally accepted standard for surface finish, machining allowance, or dimensional tolerances. The table 3.3 shows properties of gray cast iron with high carbon content, with good thermo physical characteristics and the brake disc has an isotropic elastic behavior.

Table 3.3 Thermal Properties of Disc and Pads

Material Properties	Pad	Disc
Thermal conductivity, k (w/m.℃)	5	57
Specific heat, c (J/kg.℃)	1000	460
Thermal expansion α, 10^{-6}/ ^{0}c	10	10.85

Table 3.4 Physical Constants of Atmospheric Air

Atmospheric air properties	Values
Density of dry air at 25^{o}c and 101325 Pa, ρ_a(Kg/m^3)	1.184
Dynamic viscosity of dry air at 25^{o}C, μ_a (Kgm^{-1}s^{-1})	$1.806x10^{-5}$
Specific heat of dry air, $\mathbf{c_a}$ ($\mathbf{Jkg^{-1}k^{-1}}$)	$1.00484x10^{3}$
Thermal conductivity of dry air at 25^{o}C, k_a(Wm^{-1}k^{-1})	$2.601x10^{-2}$

The thermal structural stability of the disc brake is influenced by the thermal and elastic property of cast iron materials, rate of hydraulic pressure applied on pad and the basic design for the disc rotor. Some of the thermally most important properties of disc brake rotor are as follows [22]:-

- Thermal capacitance (density and specific heat) is the ability to store the heat. Initially on braking process, a significant amount of frictional heat is stored and during short braking, this thermal capacitance is dominates.
- Thermal conductivity is the ability to re-distribute the thermal energy. During long and low intensity braking, the peak temperature is depends largely on the disc material's conductivity. However, the thermal conductivity has a little effect during short braking
- Thermal expansion coefficient (related to location of friction contact due to the thermal deformation) affects the tendency towards hot spotting and thermal disc thickness variation generation. The temperature gradients of the disc brake can cause to temporary owing to the uneven thermal expansion of the material

3.2. Analytical Analysis and Conditions

An analytical analysis expression that gives of the desired unknown quantity at any location in the body, as consequence is valid for infinite number of location in the body. For comparison of wear analysis between analytical and finite element method, the dimensions and specifications of SUV (Sport Utility Vehicle) car of model DD6470C is selected. The detail of this specification is in appendix I. Dimensions and specifications of this car are taken from previous thesis work [7]. SUV car is manufactured by Huanghai Company in China, and Bishoftu Automotive Industry imports the disassembled parts and assembles it locally. The demand of this car is increasing worldwide due to its quality in fuel economy and less expensive with an all-wheel drive or four wheel drive system. The maximum high speed set for this car is as high as 129.6km/hr that is higher than pickup car (108km/hr). This high speed of car and applied brake pressure established to be selected for the analysis of wear for it's disc brake.

Figure 3.1: Huanghai SUV car of model R425DOHC[7]

They also provide extra traction in slippery conditions and the ability to tackle at least moderate off-road terrain. Taking these in to consideration Bishoftu Automotive Industry imported the disassembled parts from Huanghai Company. The demand of this car is highly increased now days in government officials, as well as in private company.

3.2.1. Geometric and Dimensions of Disc and Pad

Dimensions of disc and pads are used for development of two dimensional and 3-D drawing. All necessary dimensions of disc-pads data and other necessary data related to this study including the SUV specification (appendix I) are taken from previous study [7].

Table 3.5 Taken Dimensions of Disc Brake Rotor and Pad Brake

Symbols	Meaning	Value
ϕ_o	The cover angle of pad (in degrees)	65
r, z, θ	Radial circumferential and axial coordinate	-
r_p	The internal radius of the pad, mm	60
R_p	External radius of the pad, mm	120
r_i	Internal radius of the disk, mm	60
R_o	External radius of the disk, mm	120
δ_d	Disk thickness, mm	24
δ_t	Vent thickness, mm	6
δ_p	pad thickness, mm	12
A_c	Surface area of the pad, mm^2	6123

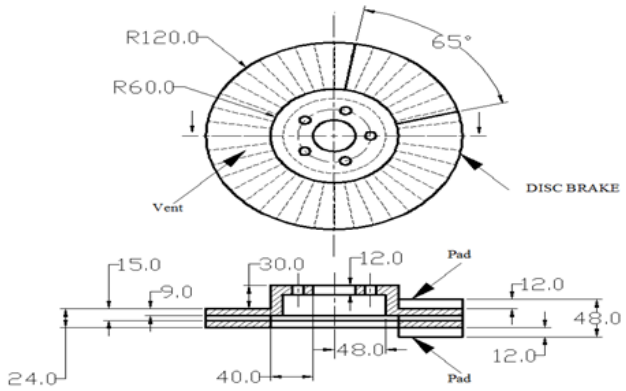

Figure 3.2: Cross Sectional Views of the Ventilated Disc and Pads

This thesis is focused on a study of ventilated disc brake in which attached on front wheel rotor of SUV Huanghai vehicle with full load of capacity with straight track for study of wear analysis. Ventilated disc and pads interaction surfaces during braking exposed to wear, so it is the main concentration of this thesis. Cylindrical coordinate system is used to describe the dimensions. Different surfaces of ventilated disc rotor and pad shown in figure 3.3 are designated by the following symbols.

Where:

Γ	Contact surface area between pads and disc (upper)
h_4	Convective heat transfer surface area of pad
h_3	Convective heat transfer surface area at external radius of disc brake
h_2	Convective heat transfer surface area at internal radius of disc brake
h_1	Surface area of disc exposed to convective heat transfer
h_5	Convective heat transfer surface area at vents
h_6	Adiabatic surface area at half of disc brake thickness
δ_p	thickness of pad
δ_d	thickness of disc
δ_t	thickness of vent
P	applied force
r_o	external radius of disc brake
r_i	internal radius of disc brake

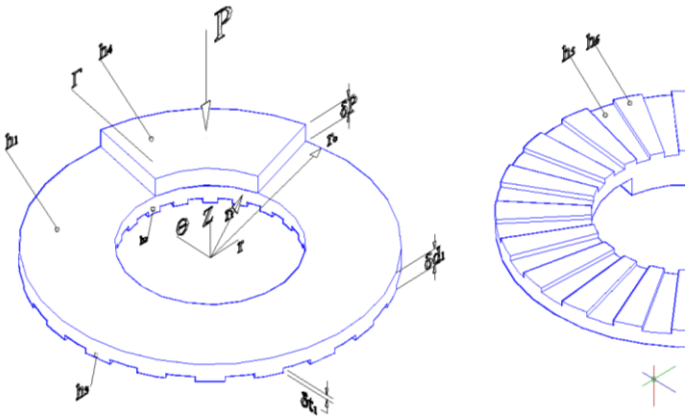

Figure 3.3: Dimensioning Ventilated Disc and Pad

3.2.2. Assumptions for Thermal-Structural Analysis

To simplify the analysis, several assumptions have also been made as follows [23].

1. The heat transfer involved for this analysis only conduction and convection process. This heat transfer radiation can be neglected in this analysis because of small amount which is 5 % to 10 % [24]. Indeed, the heat radiation only plays an important role at high temperature and low speeds.
2. The disc material is considered as homogeneous and isotropic, because Young's modulus, Poisson's ratio, and the thermal expansion coefficient are assumed to be constant for isotropic.
3. The domain is considered as axis symmetric. The temperature field and applied hydraulic pressure are symmetry with respect to the central plane of the brake disc.
4. The disc is stress free before the application of brake. Due to the application of brakes of the rotor, heat generation takes place due to friction and this temperature so generated has to be conducted across the disc across section.
5. In this analysis, the ambient temperature and initial temperature has been set to 25 °C and 30°C respectively where adopted from previous study [7].
6. Parts of disc brake rotor will apply with convection heat transfer such as cooling vanes area, outer ring diameter area and disc brake surface on which, each surface of the rotor was subjected to different values of convection heat transfer coefficient obtained from this calculations.
7. The car is not climbing or descending a hill, this makes the potential energy that can be developed by the car to be zero. Also, neglecting drag and other losses outside the brakes, and no skidding of the car tires on the road surface.

8. The radius of pad assume circular in order to get initial herztian contact pressure.
9. The pads are assumed rigid to get pressure distribution on the surface of disc brake rotor.

3.2.3. Thermal-Structural Boundary Conditions

The boundary and initial conditions of non-stationary ventilated disc brake rotor and pad as shown in Fig. 3.3 is given as follow as bellow.

$$\left.\begin{array}{l} \sigma_{zz}(r) = -p(r) \quad r \in \Gamma \\ \sigma_{rz}(r) = -\mu p(r) \quad r \in \Gamma \\ q(r,t) = -\mu v(t) p(r) \quad r \in \Gamma \end{array}\right\} \quad \text{..... (3.1)}$$

Where: $\sigma_{zz}(r)$ is the longitudinal stress as function of radial distance

$\sigma_{rz}(r)$ is the shear stress as function of radial distance

$q(r,t)$ is the heat flux as function of radial distance and time

$v(t)$ is the velocity of car with respect to time

$p(r)$ is the contact pressure along radial direction

r is radial distance

t is time

μ is *the* coefficient of friction between the brake pad and rotor

The initial and boundary condition of disc is given as shown below.

$$\left.\begin{array}{c} k_d \cdot \frac{\partial T}{\partial z} = q_d(r,t),\ z = 0\ \ r_i \le r \le R_o\ , 0 \le \theta \le 2\pi, 0 \le t \le t_s \\ k_d \cdot \frac{\partial T}{\partial z} = h_5(T_\infty - \big(T(r,z,t)\big),\ z = 9\ , r_i \le r \le R_o\ \ , 0 \le \theta \le 2\pi, t \ge 0 \\ k_d \cdot \frac{\partial T}{\partial z} = 0,\ z = 12, r_i \le r \le R_o\ , 0 \le \theta \le 2\pi, t \ge 0 \\ \int_{r_i}^{r_o} \left(\left(k_d \cdot \frac{\partial T}{\partial r} \right)_{r = \frac{r_o - r_i}{2}} \right) dr = q_{do} \\ k_d \cdot \frac{\partial T}{\partial r} = h_3\big(T_\infty - T(r,z,t)\big),\ r = R_o\ \ , 0 \le \theta \le 2\pi,\ 0 \le z \le \delta d\ \ , t \ge 0 \\ k_d \cdot \frac{\partial T}{\partial r} = -h_2\left(T_\infty - T(r,z,t)\right), r = r_i\ , 0 \le \theta \le 2\pi\ , 0 \le z \le \delta d\ , t \ge 0 \\ qA = hA(T(r,z,t) - T_\infty)\ 9 \le z \le 12, r_d \le r \le R_d\ t \ge 0 \\ T(r,\theta,z,0) = T_0\ , r_i \le r \le R_o, 0 \le \theta \le 2\pi, 0 \le z \le \delta d \end{array}\right\} \quad \text{..... (3.2)}$$

Where: $\frac{\partial T}{\partial z}$ is the partial derivative of contact temperature with respect to longitudinal direction

$\frac{\partial T}{\partial r}$ is the partial derivative of contact temperature with respect to radial direction

k_d is the thermal conductivity of disc brake, k (w/m.℃)

$T(r, z, t)$ is temperature distribution with respective to radial, longitudinal direction and time

q_{do} is heat flux of disc brake at time zero

T_∞ is ambient temperature

T_0 is initial temperature of disc brake

t_s is the stopping time during brake

The initial and boundary condition of pad is given as shown below.

$$\left.\begin{aligned} k_p \frac{\partial T}{\partial z} &= q(r,z,t),\ z = 0 \\ k_p \frac{\partial T}{\partial z} &= h_1(T(r,z,t) - T_\infty),\ z = 12 \\ k_p \frac{\partial T}{\partial r} &= h_2(T(r,z,t) - T_\infty),\ r = r_i \\ k_p \frac{\partial T}{\partial r} &= h_3(T(r,z,t) - T_\infty),\ r = r_o \end{aligned}\right\} \quad \text{..... (3.3)}$$

Where: k_p is the thermal conductivity of pad brake, k (w/m.℃)

3.3. Analytical Analysis of Contact Pressure Distribution for Structural

Contact problems are one of the challenging issues of Solid Mechanics, because contact is the main method of applying loads to a deformable body, which results in stress concentration in the most critical point in the body. More complexity of the contact problem appears when friction laws are taken into account, which leads to non-linear behavior of connected bodies. The way to carry a load between two deformable bodies is a direct contact between them. The critical point of this direct contact is the stress localization that results, and this often yields to material damage. Depending on the curvature of the bodies in contact, one can define conforming or non-conforming contacts. In the case of a non-conforming contact, the contact zone is considered negligible compared to the radii of curvature and the behavior of the contacting bodies. The resolution of the problem consists in finding the real area at the contact pressure distribution. Historically, the first development of analytical solution for contact for the frictionless contact of two elastic bodies goes back to 1881 from the paper of Heinrich Hertz [25]. Hertz developed a theory to calculate the contact area and pressure

between the two surfaces and predict the resulting compression and stress induced in the objects. This section addresses the basics of Hertzian contact stress theory and its relation to certain aspects of sliding contact problem. Contact between two continuous, non-conforming solids is initially a point or a line. Hertz contact stress theory allows for the prediction of the resulting contact area, contact pressure, compression of the bodies, and the induced stress in the bodies. Hertz for developing his theory made some simplifying assumptions, which are summarized as follows:

- Surfaces are continuous and non-conforming (i.e. initial contact is a point or a line)
- Induced strains due to contact load are small
- The material behaves elastically
- The contact is frictionless

Sliding contact usually involves the solution of both the normal problem for the contact area and the pressure, and the tangential problem for the shear stress. The tangential problem is usually more difficult to solve. If the normal problem of a contact is solved with Hertz theory, the solution and the employed method is called Hertzian, thought its tangential problem has still to be solved by some other means. If the normal problem cannot be solved with Hertz theory, it is non-Hertzian. When the geometries in contact cannot be approximated as ellipsoids or when the behavior of the body is no more elastic, numerous analytical solutions exist as well. For full sliding situations, the normal contact problem is all-sufficient since the shear generated is directly the product of the friction coefficient by the contact pressure. A spherical contact is considered, on which a normal and tangential loading are applied. The ratio between the loads has to stay below the full slip condition given by Coulomb law. Mindlin and Deresiewicz [28] went further considering a tangential loading proportional to the normal loading. And also, Lots of contact problems don't fit the assumptions listed in the previous section (Hertzian contact), i.e. a normal and frictionless contact between two semi-infinite bodies whose contacting surfaces is supposed to be paraboloids. Another type of contact configuration, which is used in this study, is at on at contact. This type of contact is called conforming contact, where the contact width is dependent of the applied contact load [26]. As depicted in Figure 3.4, this type of contact configuration is distinguished by its sharp corners, which act as stress riser in contact with other components. By assuming the plane elastic half-space hypothesis, the analytical solution for at on at contact configuration gives

rise to an asymptotic pressure distribution at contact edges [27]. The analytical solution for contact pressure distribution can be written as:

$$p(x) = \frac{F}{\pi a\sqrt{a^2 - x^2}} \quad \text{...} \; (3.4)$$

Where: F is applied force

a is the radius of flat ended punch

p(x) is contact pressure along in axial direction

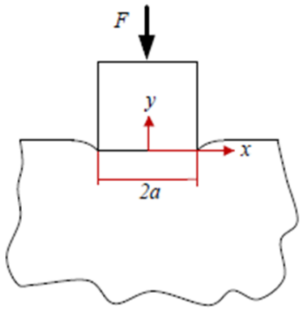

Figure 3.4: Flat on at Contact Configuration [27]

Figure 3.4 illustrates the variation of normalised contact pressure over contact interface. As it can be seen from the figure, at contact edges i.e. $x = \pm a$, the pressure distribution shows singular behaviour.

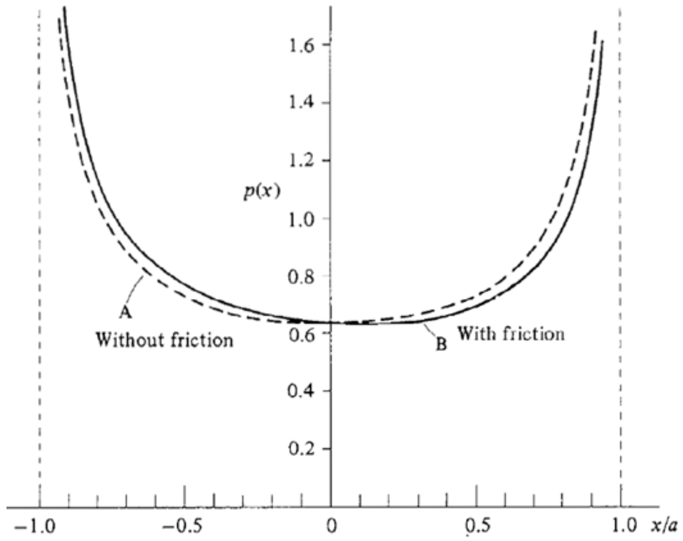

Figure 3.5: Contact Pressure Distributions for Contact Configuration [27]

The pressure peaks shown in Figure 3.5 indicate that these will create a theoretical pressure singularity at the contact edges ($x = \pm a$). The inclination of the punch, the relative modulus between the punch and half-space and the coefficient of friction at the contact affect the order

of singularity at the contact edges [29]. The presence of contact pressure singularities at the edges of contact implies that a high stress singularity will also exist here. An obvious drawback in the adoption of an elastic half-space assumption is that non-physical infinite stresses are predicted. In reality plasticity would occur in these regions. Analytical techniques are generally limited to the rigid-perfectly plastic assumption when applied to problems involving plasticity. In this case the punch has a circular section of radius a. It is pressed onto an elastic half-space with a force P. Again the surface of the punch is assumed frictionless. Contact occurs across a circle of radius a and the resulting pressure distribution (Figure 3.5) is [27]. Before analyze contact pressure during braking, we will analyze contacting force in which applied to disc brake by using the braking pressure which is give in previous thesis [7] by using this data we analyze a force applied to the disc brake. The external pressure between the disc and the pads is calculated by the force applied to the disc; for a flat track, the hydraulic pressure is as referred to [30]:

$$F_{friction} = p_b \cdot \mu \cdot A_c \quad \text{..... (3.5)}$$

This frictional force is related to the caliper clamp force as follows:

$$F_{clamp} = {}^{F_{friction}}/_{\mu}$$

Where: P_b is applied hydraulic pressure in Mpa

Ac is the surface area of the pad in contact with the disc

$F_{friction}$ is the frictional force generated by the brake pads

F_{clamp} is the clamp force generated by the caliper

Now by using the force applied to the disc brake, we will analysis the contact pressure distribution between disc brake and pad surfaces. Before executing the analytical analysis for disc brake contact pressure distribution to understand the contact behavior, it is possible to execute the same contact behavior for flat rigid axisymmetric punch (rounded edge) to flat disc interaction as shown in Figure 3.6b. Contact interaction between disc brake and pad is shown in Figure 3.6a, which is a part of the contact between flat rigid axisymmetric rounded edge on elastic flat disc as described in Figure 3.6b. But, the problem consists of an elastic punch (pad) pressed onto the rotating-disc brake, idealized as an elastic half plane (disc brake), which may, in general, be elastically dissimilar. By assumption (8) the radius of pad is denoted by a , in which, it is half of the difference between outer and inner radius of the

disc brake. This contact interaction is studied in detail by analytically using Hertz theory in the present work.

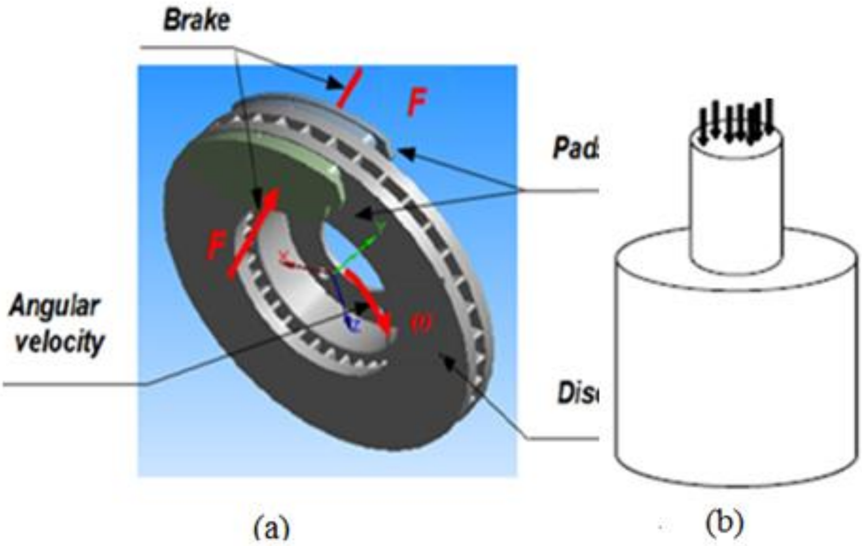

Figure 3.6: Schematic of Contact Profile of Flat Rigid Axisymmetric Punch on Flat Disc [27]

The distribution of normal pressure due to couple effect of both normal and tangential traction in which an indentation flat ended punch with a speed much less than the velocity of elastic waves, so that inertia forces can be neglected, and is sliding along the surface of the half-space from right to left, has the boundary conditions of $\bar{u}_z(r) = constant = \delta_z$, $q(r) = \mu\, p(r)$ is given by [27]:

$$p(r) = \frac{F_{clamp} \cos \pi\vartheta}{\pi a(a^2 - r^2)^{1/2}} \left(\frac{a+r}{a-r}\right)^{\vartheta} = \frac{0.999 * \quad F_{clamp}}{\pi a(a^2 - r^2)^{1/2}} \quad \ldots\ldots\ldots\ldots\ldots\ldots(3.6)$$

Where

$$\cot \pi\,\vartheta = \frac{2}{\mu}\left[\frac{\left(\frac{1-v_d}{G_d}\right)+\left(\frac{1-v_p}{G_p}\right)}{\left(\frac{1-2v_d}{G_d}\right)-\left(\frac{1-2v_p}{G_p}\right)}\right]$$

Where: v_d poisson's ratio of disc brake

v_p poisson's ratio of disc brake

$G_d = \frac{1}{2} \cdot \frac{E_d}{(1+v_d)}$

$G_p = \frac{1}{2} \cdot \frac{E_p}{(1+v_p)}$ G_d, G_p are the shear modulus of materials disc and pad respectively

E_d Modulus of Elasticity of disc brake

E_p Modulus of Elasticity of pad brake

Inoder to apply Eq. (3.6) to our problem, some modification is required. So that, the center of it is at point O as shown below Figure 3.7 and substituting value of ϑ into it and we assume that the effect of $\left(\frac{a+r}{a-r}\right)^{\vartheta}$ is small compared to other expression, so it is approximately 1, and from the above discussion we are analysed contact pressure at r=0.95a, by considering non-physical infinite stresses are predicted. Therefore, Eq. (3.6) becomes:

$$P_c = \frac{0.999* \quad F_{clamp}}{\pi a(a^2-r^2)^{1/2}} = \frac{p_d}{\left(1-\left(\frac{r}{a}\right)^2\right)^{1/2}} = 3.2p_d \text{.....(3.7)}$$

3.4. Analytical Analysis of Wear for Structural Analysis

Wear is a process of gradual removal of a material from surfaces of solids subject to contact and sliding. Damages of contact surfaces are results of wear. A modified form of ARCHARD'S equation is used here to predict the local wear depth increment for a given point within the contact as shown below:

$$dh_s = Kpds \text{ ..... (3.8)}$$

Where: K is the dimensional wear coefficient (mm^2N/m)

h_s is the wear depth by effect brake pressure (mm), & s is sliding distance

Substituting $ds = v(t)dt$, in to Eq. (3.8) in order to use ARCHARD'S equation to relate the problem.

$$dh_s = p_c k\, v(t)dt = p_c\, k\ \ \omega(t)\, r\, dt \text{ ..... (3.9)}$$

Where: $\omega(t)$ is the angular velocity of disc brake with time

Integrating equation (3.9) with respect to time, we will get:

$$\int_{h_o}^{h} dh_s = \int_{t_1}^{t_2} p_c k\ \ \omega_o \left(1-\frac{t}{t_s}\right) r\, dt \text{ ..... (3.10)}$$

Where: ω_o is the rotational speed of disc brake is calculated as follows:

$$\omega_o = \frac{V_o}{R_{tire}} \text{ ..... (3.10a)}$$

Where: V_o is the initial velocity of vehicle

R_{tire} is the tire radius of vehicle

Finally, the thickness of the worn material form disc brake with respect to brake pressure is express as follow as below:

$$h_s = 0.0141\, p_d \ [mm] \quad \text{(3.11)}$$

Wear coefficient should be noted that the wear coefficient *k* is not an intrinsic material property but is also dependent on the operating condition. The value of *k* for a specific operating condition and given pair of materials may be obtained by experiments. Also worth noting, is that measured values of wear coefficients usually have large scatter and may affect wear predictions significantly. Care should thus be taken in obtaining these values K is the wear coefficient which distinguish between the wear mechanisms by considering the area subjected to wear it is possible to express the wear displacement in terms of the contact pressure and it is often called the specific wear rate and quoted in units of mm3 N−1 m−1. For a material with a hardness H of 1 GPa (a soft steel, or a hard aluminium alloy, for example), the numerical value of k expressed in mm3 N−1 m−1 is exactly the same as the value of K. Under unlubricated sliding conditions (so-called dry sliding), it can be as high as 10−2, although it can also be as low as 10−6. Often two distinct regimes of wear are distinguished, termed 'severe' and 'mild'. Not only do these correspond to quite different wear rates (with it often above and below 10−4, respectively), but they also involve significantly different mechanisms of material loss. In metals, 'severe' sliding wear is associated with relatively large particles of metallic debris, while in 'mild' wear the debris is finer and formed of oxide particles. In the case of ceramics, the 'severe' wear regime is associated with brittle fracture, whereas 'mild' wear results from the removal of reacted (often hydrated) surface material. When hard particles are present and the wear process involves abrasion (by sliding or rolling particles) or erosion (by the impact of particles), then the highest values of K occur [31]. We can show the range of it exhibited under different conditions of wear as shown below Figure 3.7.

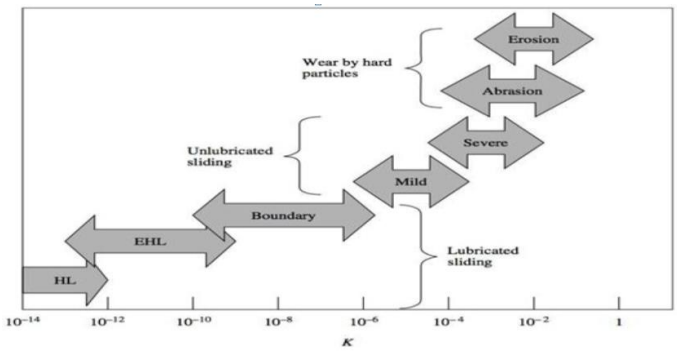

Figure 3.7: Wear Coefficient Values [31]

So far, form above explanation and research reference in the simulation the wear rate coefficient is set to k = 1.78x10−13m^3/Nm [32], we are using this value to simulate wear depth for both structural and structural-thermal analysis.

3.5. Analytical Analysis of Contact Surface Temperature for Disc Brake and pad during Braking process

Frictional heat power generated at the contact interface of a disc-pad system can be expressed as a form of heat flux given by:

$$q(r,t) = \mu V(t) p(r) \quad \text{..... (3.12)}$$

Where: V (t) time-dependent speed in which given by the following formula

$$V(t) = V_o \cdot \left(1 - {}^{t}/_{t_s}\right) \quad \text{..... (3.13)}$$

The intensity of heat flux into disc on the contact area is given by [33]:

$$q_d(r,t,z) = \gamma \frac{\emptyset_0}{2\pi} \mu\, q(r,t) \quad r_p \le r \le R_p \ , 0 \le t \le t_s \text{ ..... (3.14)}$$

The intensity of heat flux into disc on the contact is given by p_o and $p_{(r)}$ is as follow as below:

$$q_{do} = \gamma \frac{\emptyset_0}{2\pi} \mu v_o p_o = \gamma \frac{\emptyset_0}{2\pi} \mu \omega_o R_m p_o \quad \text{..... (3.15)}$$

Where: R_m is the mean radius of internal and external radius of disc brake

p_o is the contact pressure at $r = 90mm$

ω_o is angular velocity of disc brake at time equal to zero

and similarly heat flux into the pad is given below

$$q_p = (1-\gamma) \cdot q(r,t) \quad r_p \le r \le R_p \ , 0 \le t \le t_s \text{ ..... (3.16)}$$

Where: γ is the heat partitioning factor

r_p and R_p are the internal and external radius of the pad.

The heat partitioning factor representing the fraction of frictional heat flux entering the disc has the form [34]:

$$\gamma = \frac{1}{1+\sqrt{\rho_p c_p k_p / \rho_d c_d k_d}} \quad \text{...} \quad (3.17)$$

Where: ρ is the density,

c is the specific heat and

k is the thermal conductivity. They are values of disc and pad brake.

For continued braking or repeated brake applications, Eq. (3.17) assumes a more complicated form due to the convective heat transfer occurring as a result of higher brake temperature [34].In order to determine the temperature distributions; both analytical and numerical techniques have been employed. The starting point of the analysis of the temperature fields in the disc volume is the parabolic heat conduction equation given in the cylindrical coordinate system (r, θ, z)[35].

$$\left.\begin{array}{c} \frac{\partial^2 T}{\partial r^2} + \frac{\partial T}{r\partial r} + \frac{1}{r^2}\cdot\frac{\partial^2 T}{\partial \theta^2} + \frac{\partial^2 T}{\partial z^2} = \frac{1}{K_d}\left(\frac{\partial T}{\partial t} + \omega\frac{\partial T}{\partial \theta}\right), \\ r_i \le r \le R_o, 0 \le \theta \le 2\pi, 0 \le z \le \partial_d, t > 0 \end{array}\right\} \text{....................} \quad (3.18)$$

In automotive disc brakes the Peclet numbers almost always are in order 10^5 [35]. Hence the distribution of heat flow will be uniform in circumferential direction, which means that neither temperature nor heat flow will vary in θ direction nor thus the heat conduction equation reduces to:

$$\frac{\partial^2 T}{\partial r^2} + \frac{1}{r}\cdot\frac{\partial T}{\partial r} + \frac{\partial^2 T}{\partial z^2} = \frac{1}{K_d}\cdot\frac{\partial T}{\partial t} \quad r_d \le r \le R_d, 0 \le z \le \partial d, t > 0 \text{ ... ...} \quad (3.19)$$

Where: $K_d = \frac{k_d}{\rho_d c_d}$ is thermal diffusivity

3.5.1. Prediction of Convective Heat Transfer Coefficient

The computation of brake temperatures requires information on the convective heat transfer coefficient which varies with vehicle speed. In many cases it is sufficient to evaluate the some mean speed. Computer solutions make it convenient to predict brake temperatures when the heat generation or convective heat transfer coefficient is variable during the braking process. Convective heat transfer coefficient has been shown that experimental results of a cooling analysis can be represented by the product of dimensionless numbers raised to some power [36].

$$N_u = C{R_e}^m \cdot pr^{n_h} \quad \text{..} \quad (3.20)$$

Where: $N_u = \frac{h_R \cdot L_c}{k_a}$ is Nusselt number, d'less

C is heat transfer coefficient, d'less

$R_e = \frac{V\rho_a L_c}{\mu_a}$ is Reynolds number, d'less

$pr = \frac{3600 c_a \mu_a}{k_a}$ is Prandtl number, d'less

c_a is specific heat of air

h_R is convective heat transfer coefficient

k_a is thermal conductivity of air

m is heat transfer parameter, d'less

n_h is heat transfer parameter, d'less

ρ_a is density of air

μ_a is viscosity of air

L_c is characteristic length, mm

The constant C in Eq. 3.20 is a function of the geometry of the brake and assumes different values for brake drums, solid rotors, and ventilated rotors. For ventilated rotors the value of C depends upon the shape of the vanes used for ventilation. The heat transfer parameter m is a function of the type of flow, i.e., turbulent, laminar, or transition flow. For most practical cases *m* is a function of vehicle velocity and the associated brake rotor angular velocity. The heat transfer parameter n_h depends upon the thermal properties of the air. Since these properties are a function of temperature, the Prandtl number effect is nearly constant for most cases and is often included in the constant C of Eq.3.20. Ventilated disc brakes generally exhibit convective heat transfer coefficients approximately twice as large as those associated with solid discs. The cooling effectiveness associated with the internal vanes tends to dew ease somewhat for higher speeds due to the increased stagnation pressure of the air. The pumping action of the rotor is reduced as ambient air tends to enter the rotor at the front portion of brake due to vehicle speed. For estimating purposes the following relationship may be used to obtain the heat coefficient inside the vanes of the brake rotor [24, 37].

$$h_R = 0.023\left[1 + \left(\frac{d_h}{L}\right)^{0.67}\right] \times {R_e}^{0.8} pr^{0.33} \left(\frac{k_a}{d_h}\right) \quad \text{..... (3.21)}$$

Where: h_R is the heat coefficient inside the vanes of the brake rotor

$$R_e = \left(\frac{\rho_a d_h}{\mu_a}\right) V_{average}$$

d_h is hydraulic diameter, mm

L is characteristic length of vane or length of cooling vane, mm

$V_{average}$ is average velocity in vane, mm/s

Eq. 3.21 is valid for $Re > 10^4$, i.e., for turbulent flow. The hydraulic diameter is defined as the ratio of four times the cross-sectional flow area (wetted area) divided by the wetted perimeter as illustrated in Figure 3.9. For vanes with varying cross-sectional size, an average hydraulic diameter is determined from the dimensions of the inlet and outlet locations or the vane. The velocity associated with the Reynolds number is that existing in the vanes which ' not identical to the forward speed of the vehicle. For low values of velocity, laminar flow will exist in the vanes. For $Re < 10^4$ the convective heat transfer coefficient may be approximated by [24]:

$$h_R = 1.86(R_e pr)^{1/3} \cdot \left(\frac{d_h}{L}\right)^{0.33} \times \left(\frac{k_a}{d_h}\right) \quad \text{..... (3.22)}$$

For this thesis used laminar flow formulae to calculate convective heat transfer coefficient through vanes.

The average velocity through the cooling vanes can be computed by:

$$V_{average} = \frac{V_{in}+V_{out}}{2} \quad \text{..... (3.23)}$$

Where: $V_{average} = 0.052 n_r (D^2 - d^2)^{1/2}$ mm/sec

$V_{out} = V_{in} \frac{A_{in}}{A_{out}}$, mm/sec

V_{out} is the outlet velocity of the cooling vanes, mm/sec

V_{in} is the inlet velocity of the cooling vanes, mm/sec

A_{in} is the inlet area of vane, mm^2

A_{out} is the outlet area of vane, mm^2

D is the outer diameter of the rotor, mm

d is the inner diameter of the rotor, mm

n_r is the revolutions per minute of rotor, rpm

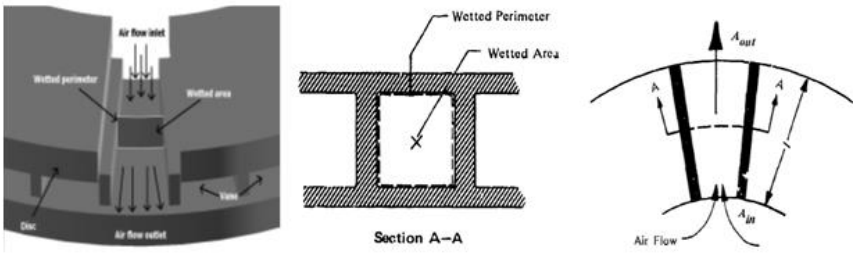

Figure 3.8: Air Flow in the Vane of Ventilated Brake Disc [24]

The convective heat transfer coefficients of the ventilated disc brake are quoted from the experiential formulas by Limpert [38]. For the solid part of the ventilated disc, the convection heat transfer coefficient associated with laminar flow can be approximated by:

$$h_R = 0.70 \frac{k_a}{D} \cdot R_e^{0.55} \quad \text{..... (3.24)}$$

Where: D is the inner or outer diameter, mm

And for $R_e > 2.4x10^5$ the flow characteristics will become turbulent and the transfer coefficient may be expressed as:

$$h_R = 0.04 \frac{k_a}{D} \cdot R_e^{0.8} \quad \text{..... (3.25)}$$

Therefore, we will apply the above formula to our problems to calculate the mean speed of the vehicle at some six different seconds starting 0 second to the last 4.5 second .So , the mean speed of vehicle, $V_m = 16.67\ m/sec.$

$$R_e = V_m \rho_a \frac{L_C}{\mu_a}$$

$$R_e = 1.262x10^4$$

$$pr = 3600 c_a \frac{\mu_a}{k_a}$$

Where: R_e is the Reynolds number and $R_e < 2.4x10^5$, therefore we use laminar formula that is:

$$h_2 = 0.70 \cdot \frac{k_a}{D_i} R_e^{0.55}$$

$$h_3 = 0.70 \cdot \frac{k_a}{D_o} R_e^{0.55}$$

3.5.2. Solve Differential Heat Equation using Non-Dimensional Parameters to Analysis Contact Temperature

Introduction of the following non-dimensional parameters simplifies the mathematical formulation of the problem.

Dimensionless temperature $\theta(r,z,t)=\frac{T(r,z,t)-T_\infty}{T_i-T_\infty}$ …… (3.26)

Dimensionless distance from the center along z-direction: $Z=\frac{z}{\frac{\delta_d}{2}}\quad 0\le Z\le 1$

A dimensionless radial position (R) is defined for convenience: $R=\frac{(r-r_i)}{(r_o-r_i)}\quad 0\le R\le 1$

Dimensionless heat transfer coefficient: $Bi=\frac{h\delta_d}{2k_d}$ (Biot-number)

Dimensionless heat transfer coefficient: $Bi=\frac{hr_0}{k_d}$ (Biot-number)

Dimensionless time: $\tau=\frac{K_d t}{L_c^2}$ (Fourier number)

With the new variables, the mathematical formulation of the heat conduction problem becomes:

$$(T_i-T_\infty)\frac{\partial^2\theta}{(r_o-r_i)^2\partial R^2}+(T_i-T_\infty)\frac{\partial\theta}{(r_o-r_i)r\partial R}+(T_i-T_\infty)\frac{4\partial^2\theta}{\delta_d^2\partial Z^2}=(T_i-T_\infty)\frac{\partial\theta}{L_c^2\partial\tau}\ \text{……}$$

(3.27a)

$$\frac{\partial^2\theta}{(r_o-r_i)^2\partial R^2}+\frac{\partial\theta}{(r_o-r_i)[(r_o-r_i)R+r_i]\partial R}+\frac{4\partial^2\theta}{\delta_d^2\partial Z^2}=\frac{\partial\theta}{L_c^2\partial\tau}\quad \text{…… (3.27b)}$$

This is subject to the following boundary and initial conditions respectively for pad and disc brake.

$$\begin{cases}(T_i-T_\infty)\dfrac{2k_p\partial\theta(0,\tau)}{\delta_p\partial Z}=q_p(r,t)\\ \dfrac{\partial\theta(1,\tau)}{\partial R}-\dfrac{(r_o-r_i)h_8\theta(1,\tau)}{k_8}=0, Bi_3=\dfrac{-(r_o-r_i)h_8}{k_p}\\ \dfrac{\partial\theta(12,\tau)}{\partial Z}+Bi_6\theta(12,\tau)=0,\ \ Bi_6=\dfrac{\delta_p h_6}{2k_p}\\ \dfrac{\partial\theta(2,\tau)}{\partial R}+\dfrac{h_7(r_o-r_i)\theta(2,\tau)}{k_p}=0, Bi_7=\dfrac{(r_o-r_i)h_7}{k_p}\end{cases}$$

$$\text{boundary condition:}\quad \begin{cases} (T_i - T_\infty)\dfrac{2k_d\partial\theta(0,\tau)}{\delta_d\partial Z} = q_d(r,t) \\ \dfrac{\partial\theta(3/4\,,\tau)}{\partial Z} = \dfrac{-\delta_d h_5\theta(3/4\,,\tau)}{2k_d} \\ \dfrac{\partial\theta(3/4\,,\tau)}{\partial Z} + Bi_5\theta(3/4\,,\tau) = 0,\;\; Bi_5 = \dfrac{\delta_d h_5}{2k_d} = 35.57 \\ (T_i - T_\infty)\dfrac{2k_d\partial\theta(1,\tau)}{\delta_d\partial Z} = 0 \\ \dfrac{\partial\theta(1,\tau)}{\partial Z} = 0 \\ \displaystyle\int_{r_i}^{r_o}\left(\frac{(T_i - T_\infty)}{(r_o - r_i)}\frac{k_d\partial\theta(1/2\,,\tau)}{\partial R}\right)dr = q_{do} \\ \dfrac{\partial\theta(0,\tau)}{\partial R} + \dfrac{h_2(r_o - r_i)\theta(0,\tau)}{k_d} = 0, Bi_2 = \dfrac{(r_o - r_i)h_2}{k_d} = 7.883 \\ \dfrac{\partial\theta(0,\tau)}{\partial R} + Bi_2\theta(0,\tau) = 0 \\ \dfrac{\partial\theta(1,\tau)}{\partial R} - \dfrac{(r_o - r_i)h_3\theta(1,\tau)}{k_d} = 0, Bi_3 = \dfrac{-(r_o - r_i)h_3}{k_d} = -3.94 \\ \dfrac{\partial\theta(1,\tau)}{\partial R} + Bi_3\theta(1,\tau) = 0 \end{cases} \quad (3.28a)$$

$$\text{initial condition:}\quad T(r,z,0) = T_i \ldots\ldots\ldots\ldots\ldots\ldots (3.28b)$$

There are several analytical and numerical techniques can be used to solve Eq.3.27. But, we will use the method of separation of variables. The dimensionless temperature function $\theta(R, Z, \tau)$ is expressed as a product of a function of R , a function of Z and a function of τ as:

$$\theta(R,Z,\tau) = F(R)G(Z)H(\tau) \;\ldots\ldots\ldots\ldots\ldots\ldots\ldots\ldots\ldots\ldots\ldots\ldots\ldots\ldots (3.29)$$

Substituting Eq. 3.29 into Eq. 3.27b and dividing by the product FGH gives:

$$\frac{\partial^2 F}{(r_o-r_i)^2 F} + \frac{\partial F}{(r_o-r_i)[(r_o-r_i)R+r_i]F} + \frac{4\partial^2 G}{\delta_d^2 G} = \frac{\partial H}{L_c^2 H} \quad \ldots\ldots\ldots\ldots\ldots\ldots\ldots\ldots (3.30)$$

Since R, Z and τ can be varied independently, the equality in Eq.3.30 can hold for any value of R, Z and τ only if Eq.3.30 is equal to a constant and it must be a negative constant will indicate by $-\lambda^2$ since a positive constant will cause the function $H(\tau)$ to increase indefinitely with time. So, *we are* setting Eq. 3.30 equal to $-\lambda^2$ gives:

$$\frac{\partial^2 F}{(r_o-r_i)^2 F}+\frac{\partial F}{(r_o-r_i)[(r_o-r_i)R+r_i]F}+\frac{4\partial^2 G}{\delta_d^2 G}+\lambda^2=0 \text{ ..... (3.31)}$$

$$\frac{\partial H}{L_c^2 H}+\lambda^2=0 \text{ ..... (3.32)}$$

and also, we are setting $\frac{4\partial^2 G}{\delta_d^2 G}=-\xi^2$ *so Eq. 3.32 become equal to :*

$$\left.\begin{aligned}\frac{\partial^2 F}{(r_o-r_i)^2 F}+\frac{\partial F}{(r_o-r_i)[(r_o-r_i)R+r_i]F}-\xi^2+\lambda^2=0 \; or\\ \frac{\partial^2 F}{(r_o-r_i)^2 F}+\frac{\partial F}{(r_o-r_i)[(r_o-r_i)R+r_i]F}=\xi^2-\lambda^2=-\varsigma^2\end{aligned}\right\} \text{ ..... (3.33)}$$

$$\frac{4\partial^2 G}{\delta_d^2 G}=-\xi^2, \quad \frac{\partial^2 G}{G}+\frac{\delta_d^2\xi^2}{4}G=0 \text{ ..... (3.34)}$$

The general solutions of Eqs.3.30 and 3.32 are given respectively as shown below.

$$H(\tau)=C_1 e^{-\lambda^2 L_c^2 \tau} \text{ ..... (3.35)}$$

$$G(Z)=C_2\, cos\left(\left(\frac{\delta_d\xi}{2}\right)Z\right)+C_3\, sin\left(\left(\frac{\delta_d\xi}{2}\right)Z\right) \text{ ..... (3.36)}$$

In order to solve eqs.3.30, we are substituting internal and external radii of disc brake into it, and then rearrange some variables we will get:

$$(R+1)\partial^2 F+\partial F+(R+1)60^2\varsigma^2 F=0 \text{ ..... (3.37)}$$

This has a regular singular point at $R=-1$, so our conventional application of the method of Frobenius is to seek a solution:

$$F(R)=\sum_{n=0}^{\infty} a_n(R+1)^{\varphi+n}$$

Where: φ is representing the indicial root of eqs.3.34.

However, it is often more convenient to transform the original equation so that the ′standard ′ power series, i.e. equivalently about $R=0$,can be invoked. To do this, we write $F(R)=f(R+1)=f(W), where\ W=R+1$, and then we obtain:

$$W\partial^2 f+\partial f+60^2\varsigma^2 W f=0 \text{ ..... (3.38)}$$

This equation has a regular singular point at $W=0, (i.e. R=-1)$, and so we may seek a solution:

$f(W)=\sum_{n=0}^{\infty} a_n(W)^{\varphi+n}$ $(a_0\neq 0)$, the standard form for power series and then we obtain:

$$\partial f=\sum_{n=0}^{\infty} a_n(\varphi+n)(W)^{\varphi+n-1}$$

$$\partial^2 f = \sum_{n=0}^{\infty} a_n(\varphi+n)(\varphi+n-1)(W)^{\varphi+n-2}$$

Substituting the second, first and the function itself of f (W) into eqs.3.38 and so the equation becomes:

$$W\sum_{n=0}^{\infty} a_n(\varphi+n)(\varphi+n-1)(W)^{\varphi+n-2} + \sum_{n=0}^{\infty} a_n(\varphi+n)(W)^{\varphi+n-1} + 60^2\varsigma^2 W\sum_{n=0}^{\infty} a_n(W)^{\varphi+n} = 0$$

It is convenient to introduce new dummy counters into each summation, so that each term now takes the form $(W)^{\varphi+m}$ – this is the essential man oeuvre in simplifying an organizing the calculation. Thus in the first and second series we write n −1 = m, and in the third we simply set n + 1 = m; we then obtain:

$$\sum_{m=-1}^{\infty} a_{m+1}(\varphi+m+1)(\varphi+m)(W)^{\varphi+m} + \sum_{m=-1}^{\infty} a_{m+1}(\varphi+m+1)(W)^{\varphi+m} + 60^2\varsigma^2\sum_{m=0}^{\infty} a_{m-1}(W)^{\varphi+m} = 0$$

This equation can be rearranged to give:

$$\sum_{m=-1}^{\infty} a_{m+1}(\varphi+m+1)^2 W^{\varphi+m} + 60^2\varsigma^2\sum_{m=0}^{\infty} a_{m-1}W^{\varphi+m} = 0$$

This can now be expressed as:

$$a_0\varphi^2 W^{\varphi-1} + a_1(\varphi+1)^2 W^{\varphi} + \sum_{m=1}^{\infty}\{a_{m+1}(\varphi+m+1)^2 + 60^2\varsigma^2 a_{m-1}\}W^{\varphi+m} = 0$$

and this is an identity for all W if

$$a_0\varphi^2 = 0;\ a_1(\varphi+1)^2 = 0;\ a_{m+1}(\varphi+m+1)^2 + 60^2\varsigma^2 a_{m-1} = 0\ \ (m = 1,2,\dots)$$

But $a_0 \neq 0$, so $\varphi = 0$ (repeated roots) and then $a_1 = 0$; this leaves $a_{m+1} = \frac{-60^2\varsigma^2 a_{m-1}}{(m+1)^2}$ $(m = 1,2,\dots)$, with implies that $0 = a_1 = a_3 = a_5 = \cdots$. otherwise we obtaion $a_2 = \frac{-60^2\varsigma^2 a_0}{2^2}$; $a_4 = \frac{-60^2\varsigma^2 a_2}{4^2} = \frac{60^4\varsigma^4 a_0}{4^2 2^2}$, etc., . So $a_n = \frac{(6o\varsigma)^{2n}(-1)^n}{2^{2n}\,(n!)^2}\mathrm{a}_0$ (n = 0,1,2, …). which provides one solution of f1(W):

$$f1(W) = \sum_{n=0}^{\infty} a_n W^{2n} = \sum_{n=0}^{\infty} \frac{(60\varsigma)^{2n}(-1)^n}{2^{2n}\,(n!)^2} a_0\, W^{2n} \quad \text{..... (3.39)}$$

Multiply eqs.3.36 by $\frac{(2n)!}{(2n)!}$ and $\frac{(2n+1)!}{(2n+1)!}$, so we will get:

$$f1(W) = \sum_{n=0}^{\infty} \frac{(60\varsigma)^{2n}(-1)^n}{2^{2n}\,(n!)^2} a_0 W^{2n} \cdot \frac{(2n)!}{(2n)!} = \sum_{n=0}^{\infty} \frac{(2n)!}{2^{2n}\,(n!)^2} a_0 \cdot cos(60\varsigma W)$$

Where: $cos(60\varsigma W) = \frac{(60\varsigma)^{2n}(-1)^n}{(2n)!} W^{2n}$

Since the roots are repeated or double, then a second solution must necessarily take the form:

$$f2(W) = Wf1(W) = \sum_{n=0}^{\infty} \frac{(2n+1)!}{2^{2n}\,(n!)^2} a_0 sin(60\varsigma W) = \sum_{n=0}^{\infty} \frac{(2n)!}{2^{2n}\,(n!)^2} a_0 \cdot s\,in(60\varsigma w)$$

Where: $sin(60\varsigma W) = \frac{(60\varsigma)^{2n}(-1)^n}{(2n+1)!} W^{2n+1}$

The complete, general solution can therefore be written as:

$$f(W) = C_4 f1(W) + C_5 f2(W)$$

$$= C_4 \sum_{n=0}^{\infty} \frac{(2n)!}{2^{2n}\,(n!)^2} a_0\, cos(60\varsigma W) + C_5 \sum_{n=0}^{\infty} \frac{(2n+)!}{2^{2n}\,(n!)^2} a_0\, s\,in(60\varsigma W)$$

But , $W = R + 1$, finally we will have $F(R)$:

$$F(R) = C_4 \sum_{n=0}^{\infty} \frac{(2n)!}{2^{2n}\,(n!)^2} a_0\, cos\big(60\varsigma(R+1)\big) + C_5 \sum_{n=0}^{\infty} \frac{(2n+)!}{2^{2n}\,(n!)^2} a_0\, s\,in\big(60\varsigma(R+1)\big)$$

Therefore, substituting the value of F(R) , G(Z)and H(τ) into Eqs.3.29. Then we will have:

$$\theta(R,Z,\tau) = \Big(C_4 \sum_{n=0}^{\infty} \frac{(2n)!}{2^{2n}\,(n!)^2} a_0\, cos\big(60\varsigma(R+1)\big) + C_5 \sum_{n=0}^{\infty} \frac{(2n+1)!}{2^{2n}\,(n!)^2} a_0\, s\,in\big(60\varsigma(R+1)\big)\Big)\Big(C_2\, cos\Big(\Big(\frac{\xi\delta_d}{2}\Big)Z\Big) + C_3\, sin\Big(\Big(\frac{\xi\delta_d}{2}\Big)Z\Big)\Big)\big(C_1 e^{-\lambda^2 L_c^2 \tau}\big) \quad \text{..... (3.40)}$$

Multiply each term and simplify Eq. 3.40. and it becomes:

$$\theta(R,Z,\tau) =$$

$$\Big[C_1C_2C_4 \sum_{n=0}^{\infty} \frac{(2n)!}{2^{2n}\,(n!)^2} cos\big(60\varsigma(R+1)\big)\, cos\Big(\Big(\frac{\xi\delta_d}{2}\Big)Z\Big) + C_1C_3C_4 \sum_{n=0}^{\infty} \frac{(2n)!}{2^{2n}\,(n!)^2} cos\big(60\varsigma(R+1)\big)\, sin\Big(\Big(\frac{\xi\delta_d}{2}\Big)Z\Big) + C_1C_2C_5 \sum_{n=0}^{\infty} \frac{(2n+)!}{2^{2n}\,(n!)^2} a_0\, s\,in\big(60\varsigma(R+1)\big)\, cos\Big(\Big(\frac{\xi\delta_d}{2}\Big)Z\Big) + C_1C_4C_5 \sum_{n=0}^{\infty} \frac{(2n+)!}{2^{2n}\,(n!)^2} a_0\, s\,in\big(60\varsigma(R+1)\big)\, sin\Big(\Big(\frac{\xi\delta_d}{2}\Big)Z\Big)\Big] e^{-\lambda^2 L_c^2 \tau} \quad \text{..... (3.41)}$$

Let $H_1 = C_1C_2C_4, H_2 = C_1C_3C_4, H_3 = C_1C_2C_5,\ H_4 = C_1C_4C_5$

Where H_1, H_2, H_3 and H_4 are integral constants. To find , differentiate Eq.3.41 once with respect to Z and substituting into boundary eqs.3.28a that are related to Z as follow as:

$$\frac{\partial\theta(R,0,\tau)}{\partial Z} =$$

$$\Big[-\frac{\xi\delta_d}{2} H_1 \sum_{n=0}^{\infty} \frac{(2n)!}{2^{2n}\,(n!)^2} cos\big(60\varsigma(R+1)\big)\, sin\left(\left(\frac{\xi\delta_d}{2}\right)Z\right) + \frac{\xi\delta_d}{2} H_2 \sum_{n=0}^{\infty} \frac{(2n)!}{2^{2n}\,(n!)^2} cos\big(60\varsigma(R+1)\big)\, cos\left(\left(\frac{\xi\delta_d}{2}\right)Z\right) -$$

$$\frac{\xi\delta_d}{2} H_3 \sum_{n=0}^{\infty} \frac{(2n+1)!}{2^{2n}\,(n!)^2} a_0\, s\,in\big(60\varsigma(R+1)\big)\, sin\left(\left(\frac{\xi\delta_d}{2}\right)Z\right) + \sum_{n=0}^{\infty} \frac{(2n+1)!}{2^{2n}\,(n!)^2} a_0\, s\,in\big(60\varsigma(R+1)\big)\, sin\left(\left(\frac{\xi\delta_d}{2}\right)Z\right) + cos\left(\left(\frac{\xi\delta_d}{2}\right)Z\right)\Big]\, e^{-\lambda^2 L_c^2 \tau} \quad \text{.......................................} \; (3.42)$$

So, $\mathrm{k_d}\frac{2}{\xi\delta_\mathrm{d}}(\mathrm{T_i}-\mathrm{T_\infty})(\partial\theta(\mathrm{R},0,\tau)/\,\partial\mathrm{Z}) = \mathrm{q_d}(\mathrm{r},\mathrm{t})$

This simplification implies that

$$H_2 = \frac{q_d(r,t)}{(T_i-T_\infty)\xi k_d \sum_{n=0}^{\infty}\frac{(2n)!}{2^{2n}\,(n!)^2} cos\big(60\varsigma(R+1)\big)e^{-\lambda^2\tau}} - \frac{\sum_{n=0}^{\infty}\frac{(2n+1)!}{2^{2n}\,(n!)^2}}{\sum_{n=0}^{\infty}\frac{(2n)!}{2^{2n}\,(n!)^2}} tan\,60\varsigma(R+1)H_4 \quad \text{......} \; (3.43)$$

And also applying the convection boundary condition to find the value of H_2 and H_4 .

$$\frac{\partial\theta(3/4,0)}{\partial Z} + Bi_5\theta(3/4\,,0) = 0$$

$$-\frac{\xi\delta_d}{2} H_1 \sum_{n=0}^{\infty} \frac{(2n)!}{2^{2n}\,(n!)^2} \cos\big(60\varsigma(R+1)\big) \sin\left(\left(\frac{\xi\delta_d}{2}\right) {}^3\!/_4\right) + \frac{\xi\delta_d}{2} H_2 \sum_{n=0}^{\infty} \frac{(2n)!}{2^{2n}\,(n!)^2} \cos\big(60\varsigma(R+1)\big) \cos\left(\left(\frac{\xi\delta_d}{2}\right) {}^3\!/_4\right) -$$

$$\frac{\xi\delta_d}{2} H_3 \sum_{n=0}^{\infty} \frac{(2n+1)!}{2^{2n}\,(n!)^2} a_0\, s\,in\big(60\varsigma(R+1)\big) \sin\left(\left(\frac{\xi\delta_d}{2}\right) {}^3\!/_4\right) + \frac{\xi\delta_d}{2} H_4 \sum_{n=0}^{\infty} \frac{(2n+1)!}{2^{2n}\,(n!)^2} a_0\, \mathrm{s}\,in\big(60\varsigma(R+1)\big) \cos\left(\left(\frac{\xi\delta_d}{2}\right) {}^3\!/_4\right) +$$

$$Bi_5\Big[H_1 \sum_{n=0}^{\infty} \frac{(2n)!}{2^{2n}\,(n!)^2} \cos\big(60\varsigma(R+1)\big) \cos\left(\left(\frac{\xi\delta_d}{2}\right) {}^3\!/_4\right) + H_2 \sum_{n=0}^{\infty} \frac{(2n)!}{2^{2n}\,(n!)^2} \cos\big(60\varsigma(R+1)\big) \sin\left(\left(\frac{\xi\delta_d}{2}\right) {}^3\!/_4\right) + H_3 \sum_{n=0}^{\infty} \frac{(2n+)!}{2^{2n}\,(n!)^2} a_0\, \mathrm{s}\,in\big(60\varsigma(R+1)\big) \cos\left(\left(\frac{\xi\delta_d}{2}\right) {}^3\!/_4\right) +$$

$$H_4 \sum_{n=0}^{\infty} \frac{(2n+)!}{2^{2n}\,(n!)^2} a_0\, \mathrm{s}\,in\big(60\varsigma(R+1)\big) \sin\left(\left(\frac{\xi\delta_d}{2}\right) {}^3\!/_4\right)\Big] = 0 \quad \text{....................} \; (3.44)$$

And also , we have symmetric boundary condition at half of the disc. So that ,

$$\frac{\partial\theta(R,1,\tau)}{\partial Z} = 0$$

$$-\frac{\xi\delta_d}{2}H_1\sum_{n=0}^{\infty}\frac{(2n)!}{2^{2n}\,(n!)^2}\cos\big(60\varsigma(R+1)\big)\sin\left(\left(\frac{\xi\delta_d}{2}\right)*1\right)+\frac{\xi\delta_d}{2}H_2\sum_{n=0}^{\infty}\frac{(2n)!}{2^{2n}\,(n!)^2}\cos\big(60\varsigma(R+1)\big)\cos\left(\left(\frac{\xi\delta_d}{2}\right)*1\right)-$$

$$\frac{\xi\delta_d}{2}H_3\sum_{n=0}^{\infty}\frac{(2n+1)!}{2^{2n}\,(n!)^2}a_0\,s\,in\big(60\varsigma(R+1)\big)\sin\left(\left(\frac{\xi\delta_d}{2}\right)*1\right)+\frac{\xi\delta_d}{2}H_4\sum_{n=0}^{\infty}\frac{(2n+1)!}{2^{2n}\,(n!)^2}a_0\,s\,in\big(60\varsigma(R+1)\big)\cos\left(\left(\frac{\xi\delta_d}{2}\right)*1\right) \quad \text{..... (3.45)}$$

Substituting H_2 into Eqs.3.44 and 3.45 and Simplify , we will get:

$$H_2=\frac{q_d(r,t)}{2(T_i-T_\infty)\xi k_d\sum_{n=0}^{\infty}\frac{(2n)!}{2^{2n}\,(n!)^2}\cos\big(60\varsigma(R+1)\big)e^{-\lambda^2L_c^2\tau}}$$

$$H_4=\frac{q_d(r,t)}{2(T_i-T_\infty)k\xi_d\sum_{n=0}^{\infty}\frac{(2n+1)!}{2^{2n}\,(n!)^2}s\,in\big(60\varsigma(R+1)\big)e^{-\lambda^2L_c^2\tau}}$$

$$-Bi_5=\frac{\xi\delta_d}{2}\left[\frac{tan\left(\frac{\xi\delta_d}{2}\right)-tan\left(\frac{3\xi\delta_d}{8}\right)}{1+tan\left(\frac{3\xi\delta_d}{8}\right)tan\left(\frac{\xi\delta_d}{2}\right)}\right] \quad \text{..... (3.46)}$$

Simplifying Eq.3.46 by using trigonometric identity and some rearrangement terms, we will get:

$$-Bi_5=\frac{\xi\delta_d}{2}tan\left(\frac{\xi\delta_d}{8}\right) \quad \text{..... (3.47)}$$

To solve Eq. (3.47), we use Newton Raphson iteration method. So,

$$\xi=\frac{41.94}{\delta_d}$$

Where the arbitrary constants are now H_1 and H_3 are determined from boundary conditions. Since , we are focus on surface temperature of disc brake during brake. At the $(Z=0)$ Eq.3.45 is reducing to:

$$\theta(R,\tau)=\left[H_1\sum_{n=0}^{\infty}\frac{(2n)!}{2^{2n}\,(n!)^2}cos\big(60\varsigma(R+1)\big)+H_3\sum_{n=0}^{\infty}\frac{(2n+1)!}{2^{2n}\,(n!)^2}a_0\,s\,in\big(60\varsigma(R+1)\big)\right]e^{-\lambda^2L_c^2\tau} \quad \text{..... (3.48)}$$

We have three unknown constants and also three boundary conditions along radial directions. So, we will determine these constants as follow as below:

$$\frac{\partial\theta(1,\tau)}{\partial R}+Bi_2\theta(1,\tau)=0$$

$$-H_1\sum_{n=0}^{\infty}\frac{(2n)!}{2^{2n}\,(n!)^2}60\varsigma\,sin(60\varsigma*1)+H_3\sum_{n=0}^{\infty}\frac{(2n+)!}{2^{2n}\,(n!)^2}60\varsigma cos(60\varsigma)$$

$$+Bi_2\left(H_1\sum_{n=0}^{\infty}\frac{(2n)!}{2^{2n}\,(n!)^2}\,cos(60\varsigma*1)+H_3\sum_{n=0}^{\infty}\frac{(2n+1)!}{2^{2n}\,(n!)^2}sin(60\varsigma*1)\right)=0$$

Simplify this will get:

$$H_1=-\left(\frac{60\varsigma+B_{i2}tan(60\varsigma)}{-60\ \varsigma tan(60\varsigma)+B_{i2}}\right)\frac{K_2}{K_1}H_3 \quad \text{..... (3.49)}$$

$Where:\quad K_2=\sum_{n=0}^{\infty}\frac{(2n+1)!}{2^{2n}\,(n!)^2}$ and $K_1=\sum_{n=0}^{\infty}\frac{(2n)!}{2^{2n}\,(n!)^2}$

And also we have boundary condition at $R=1\ or\ W=2$. so,

$$\frac{\partial f(2,\tau)}{\partial W}+Bi_3f(2,\tau)=0$$

$$-60\,\varsigma K_1H_1\sin(120\varsigma)+60\varsigma\,K_2H_3\cos(120\,\varsigma)+Bi_3(K_1H_1\cos(120\varsigma)+K_2H_3\sin(120\varsigma))=0$$

Also simplify the above expression, we will get:

$$H_3=\left(\frac{60\,\varsigma\,tan(120\,\varsigma)-Bi_3}{60\varsigma\ +Bi_3\,tan(120\varsigma)}\right)\frac{K_1}{K_2}H_1 \quad \text{..... (3.50)}$$

In order to solve for value of ς equate Eqs.3.49 and 3.50 substituting the values of Bi_2, $Bi_3, let\ \beta=60\varsigma$ and rearrange terms. So that we will get:

$$\beta^2(tan\,2\beta-tan\,\beta)+11.823\beta\,tan\,\beta\,tan\,2\beta+31.06(-tan\,2\beta+tan\,\beta)+11.823\beta=0 \quad \text{.....(3.51)}$$

We are also use Newton Raphson iteratation method to solve Eq.3.51 and therefore the value of ς is determined that is $\varsigma=\frac{14.966}{60}$:

Finally we will determine the constants H_1 and H_3 from the third boundary condition as shown below:

$\int_{r_i}^{r_o}\left(\frac{(T_i-T_\infty)}{(r_o-r_i)}\frac{k_d\partial f(3/2,0)}{\partial W}\right)dr=q_{do}$ So, this implies that:

$$\frac{\partial f(3/2,\tau)}{\partial W}=\frac{q_{do}}{(T_i-T_\infty)k_d}$$

$$-60\varsigma K_1H_1\,sin(60\varsigma*3/2)+60\varsigma K_2H_3\,cos(60\varsigma*3/2)=\frac{q_{do}}{(T_i-T_\infty)k_d} \quad \text{..... (3.52)}$$

Since $a_o\neq 0$, we can take any number different from zero. So, $a_o=1$

Substituting the value from Eq.3.51 into eq. 3.52 and simplify it. We have

$$H_1 = \frac{3.6345 * 10^{-5} p_d}{K_1} \quad and \qquad H_2 = \frac{-9.668 * 10^{-5} p_d}{K_2}$$

Substituting the values of H_1 and H_2 into equ3.45 then we will have:

$$\theta(R,\tau) = \left[3.6345 * 10^{-5} p_d \cos\left(60\varsigma(R+1)\right) - 9.668 * 10^{-5} p_d \sin\left(60\varsigma(R+1)\right)\right] \text{.. (3.53)}$$

Substituting dimensionless parameter by dimensional parameter, then we will get that:

$$\theta(r,t) = \left(3.6345 * 10^{-5} p_d \cos\left(14.966(\left(\frac{r-r_i}{r_o-r_i}\right)+1\right) - 9.668 * 10^{-5} p_d \sin\left(14.966(\left(\frac{r-r_i}{r_o-r_i}\right)+1\right)\right)\left(e^{-\lambda^2 \alpha_d t}\right) \text{......... (3.54)}$$

But, we have dimensionless parameter Eq.3.26 substituting into Eq.3.54and also substituting $\lambda^2 = \varsigma^2 + \xi^2$. Simplify Eq.3.54 by inserting all given parameters.

$$T(r,t) = T_\infty + \left(18.173 * 10^{-5} p_d \cos\left(14.966(\left(\frac{r-r_i}{r_o-r_i}\right)+1\right) - 48.34 * 10^{-5} p_d \sin\left(14.966(\left(\frac{r-r_i}{r_o-r_i}\right)+1\right)\right)\left(e^{-0.08445t}\right) \text{......... (3.55)}$$

In order to calculate the total temperature, we must add initial temperature Eq.3.55 and when time is increasing the total temperature is decreasing, so that it is maximum at steady state condition. It is given by:

$$T(r) = 55°\text{C} + \left(18.173 * 10^{-5} p_d \cos\left(\frac{14.966r}{60}\right) - 48.34 * 10^{-5} p_d \sin\left(\frac{14.966r}{60}\right)\right) \text{...... (3.56)}$$

Where: T(r) is the total temperature distribution for disc brake

In order to calculate, the maximum contact temperature for disc brake, differential Eq.3.56 with respect to r and then equate it to zero. Then after Newton Raphson's iteration method, we will get the value for $r = 95.859mm$. After that, we are substituting these values into Eq.3.56 and after same simplification; we get relationship disc temperature with brake pressure as shown below:

$$T_c(disc) = 516.43 p_d \ [°\text{C}] \text{......... (3.57)}$$

By using the same procedure and thermal properties of pad brake is followed to calculate the contact temperature and relationship to brake pressure for it as shown below:

$$T_c(r) = \left(2.133 * 10^{-3} p_d cos\left(\frac{19.4625r}{60}\right) - 1.927 * 10^{-3} p_d sin\left(\frac{19.4625r}{60}\right)\right) \quad \text{..... (3.58)}$$

Simplified Eq.3.58 at disc brake maximum contact temperature value that is $r = 95.859mm$ and substituting this value into it.

$$T_c(pad) = 2614.287 p_d \quad [℃] \text{..... (3.59)}$$

3.6. Analytical Analysis of Contact Pressure Distribution for Thermal-Structural Effects

Tian and Kennedy [39] developed an approximate analytical solution for the steady-state maximum temperature rise of a sphere sliding on a flat in the elastic regime of deformation. Normal load and sliding velocity are assumed to be constant during the contact between the sphere and the flat. The steady-state maximum temperature rise at the contact interface is given by Tian and Kennedy [39] as:

$$T_c = \frac{1.31 a_t \, \mu \, P_t \, V_o}{k_d \sqrt{1.2344 + P_{ed}} + K_p \sqrt{1.23344 + P_{ep}}} \quad \text{..... (3.60)}$$

Where: P_t is contact pressure with the effect of brake pressure and temperature

a_t is the contact radius of temperature effect, the contact radius which will be obtained by [40].

$$a_t = \left(\frac{3.848 k_d (1 - v_d)}{\mu \omega_o \alpha_d (1 + v_d) G_d}\right)^{1/2} \text{..... (3.61)}$$

Pe is the Peclet number defined as:

$$P_e = \frac{V_o \rho_d c_d a_t}{2 k_d} \quad \text{..... (3.62)}$$

Substituting all given values form tables and also simplifying Eq.3.60, then we will get the relationship between contact pressure and contact temperature as shown below:

$$P_t = 56 p_b \quad [MPa] \text{..... (3.63)}$$

3.7. Analytical Analysis of Wear for Thermal-Structural Effects

The sliding contact between the pad and disc causes rise of temperature for both objects. This rise temperature also causes to contact pressure increase as shown given by Eq.3.60. The same assumption, wear model, procedure and wear coefficient were taken as Eq.3.10 used to estimate the thickness of the worn material form disc surface as follow as:

$$\int_{h_o}^{h} dh_t = \int_{t_1}^{t_2} p_t k\ \omega_o \left(1 - \frac{t}{t_s}\right) r\ dt \quad \text{..... (3.65)}$$

Substituting value of p_t from Eq.3.64 in to Eq.3.65 and integrate it with respect to time. Then we will have wear depth with temperature effect respect to brake pressure:

$$h_t = 0.197 p_d \ \ [mm] \quad \text{..... (3.66)}$$

Where: h_t is the wear depth by the effect of both temperature and pressure

3.8. Analytical Analysis of Von Misses Stress for Structural Effect

The maximum distortion energy theory, also known as the von misses theory, was proposed by M.T.Huber in 1904 and further developed by R.von Misses (1913).In this theory failure by yielding occurs when at any point in the body, the distortion energy per unit volume in a state of combined stress becomes equal to that associated with yielding in a simple tension test is this gives [41]:

$$\sigma_e = [(\sigma_1 - \sigma_2)^2 + (\sigma_2 - \sigma_3)^2 + (\sigma_3 - \sigma_1)^2]^{1/2} = \frac{s_y}{n} \quad \text{..... (3.67)}$$

Where: σ_e is von mises stress

σ_1, σ_2 and σ_3 are principal stress

s_y is yield strength

n is factor of safety

The maximum von misses stresses without effect of temperature is analysis starting from identifying of applied loads on disc-pad brake structures as shown in Figure.3.6 (a). So that we will analysis stress normal direction, torsion and shear directions.

$$\sigma_{zz} = \frac{F}{\pi a \delta_d} = \frac{2143.05 p_b}{3.14*0.03*0.024} = 0.95 p_b Mp_a \text{..... (3.68a)}$$

$$\sigma_{zrS} = \frac{F}{\pi a^2} = \frac{2143.05 p_b}{3.14*0.03^2} = 0.76 p_b Mp_a \text{..... (3.68b)}$$

$$\sigma_{zrT} = \frac{r_m F}{\pi a^2 \delta_d} = \frac{0.09*2143.05 p_b}{3.14*0.03*0.03*0.024} = 2.844 p_b Mp_a \text{..... (3.68c)}$$

Where: σ_{zz} is the stress normal direction

σ_{zrS} is the stress shear direction

σ_{zrT} is the stress torsion direction

The combined torsion and shear stresses by using vectors addition since they are the same type. Therefore, we have:

$$\sigma_{zr} = \sigma_{zrS} + \sigma_{zrT} = 3.604 p_b Mp_a \text{ ..... (3.68d)}$$

Since, there is no applied force in the radial direction, therefore stress in this direction is zero.

Substituting all stress into eqs.3.63 and simplifying it. Then we will get the von misses stress, σ_e for the axisymmetric analysis is defined as:

$$\sigma_{es} = \sqrt{(\sigma_{zz}^2 + 3\sigma_{zr}^2)} = 6.314 p_b Mp_a \text{ ..... (3.69)}$$

Where: σ_{es} is von misses analysis by structural effect

3.9. Analytical Analysis of Von Misses Stress for Thermal-Structural Effects

To evaluate the von misses stresses caused by temperature effect, the elastic von Misses stress (σ_e) is defined in equation 3.66 below was considered, since this parameter, which combines the three principal stresses, was assumed to determine yield (onset of plastic deformation) in metals:

$$\sigma_{et} = \frac{1}{\sqrt{2}}[(\sigma_r - \sigma_\theta)^2 + (\sigma_\theta - \sigma_z)^2 + (\sigma_z - \sigma_r)^2]^{1/2} \text{ ..... (3.70)}$$

Where: σ_{et} is the von misses stress analysis for thermal and structural effects

σ_r is radial stress

σ_θ is tangential stress

σ_z is normal stress

The constraint pressure generated at the interface of the hat and rotor is given by [41].

$$c_p = \alpha_d \Delta T E_d \left[\left(\frac{r_i^2 + r_o^2}{r_i^2 - r_o^2}\right) + 1\right]^{-1} \text{ ..... (3.71a)}$$

Where: c_p is the constraint pressure

This constraint pressure generates stresses in tangential and radial direction according to [36]:

$$\sigma_\theta = \frac{-c_p r_0^2 (r_i^2 + r^2)}{r^2 (r_i^2 - r_o^2)} = 2.258(GPa) \text{ ..... (3.71b)}$$

$$\sigma_r = \frac{c_p r_0^2 (r_i^2 - r^2)}{r^2 (r_i^2 - r_o^2)} = -0.037 pd(GPa) \text{ ..... (3.71c)}$$

But, the radial and tangential stresses are maximum at inner radius of the disc brake due to stress concentration factor. The presence of discontinuities (such as hole in a plate) alters the

stress distribution causing higher stress near the discontinuity [42]. Any types of discontinuity (holes, shoulder, notch, inclusion) serve as a stress raises where it increase stress in the vicinity of discontinuity as shown figure below.

1. Stress concentration occurs at three region in which stress raisers are present, and a stress concentration factor (K_t) is used to relate the actual maximum stress at the discontinuity to the nominal stress without the discontinuity.

$$K_t = \frac{actual\ maximum\ stress}{normal\ stress} = \frac{\sigma_{max}}{\sigma_o}$$

2. Stress concentration factors are independent of the material properties (as long as the material is in the linear elastic region). They depend only on the type of discontinuity and the geometry. One of the theoretical stress concentration factors is that of an elliptical hole in an infinite plate loaded in tension which is given as: $K_t = 1 + \frac{2b}{a}$

Thus, if the hole is circular (a=b) in an infinite plate then $K_t = 3$.

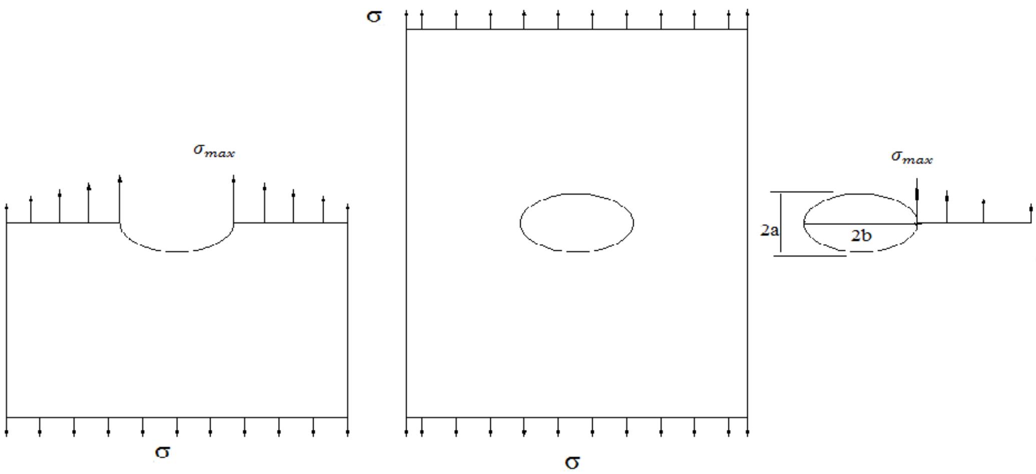

Figure 3.9: stress concentration factor to relate maximum stress to nominal stress [42]

As discuss above, we are used stress concentration factor for radial and tangential stress. So that, the stresses for radial and tangential direction will be multiply by factor of 3. Since disc brake is circular geometry type. Simplified Eq. 3.70 by substituting the above stress, then the von misses stress with respect to brake pressure will be given:

$$\sigma_{et} = 6.83 p_b \ (GPa) \quad \text{..} \quad (3.72)$$

Chapter Four

4. Finite Element Methods and Conditions

4.1. Introduction

A computerized method for predicting how a product reacts to real-world forces, vibration, heat, fluid flow and other physical effects is called finite element analysis. As finite elements analysis has become more accessible, many researchers have looked for ways to use it to calculate wear. Each has their own unique details, but the general formula is to alternate between a finite elements analysis to determine pressures and calculate of wear which adjust the model [44, 45, 46].The engineering simulation software developed by United States called ANSYS Workbench platform which is subsidiary part of ANSYS 14.0 is used here. ANSYS Workbench was chosen as the FEA software package because of its ability to accept a 3D computer aided design (CAD) model. The program also allows for the accurate placement of contact temperature and brake pressures, in addition to the modeling of contact surfaces.

4.1.1. Finite Element Methods

The finite element method is numerical analysis technique for obtaining approximate solutions to a wide variety of engineering problems. Because of its diversity and flexibility as an analysis tool, it is receiving much attention in almost every industry. In more and more engineering situation today, we find that it is necessary to obtain approximate solutions to obtain than exact to closed solution. The finite element method has become a powerful tool for the numerical solutions of a wide range of engineering problems. It has been developed simultaneously with the increasing use of the high-speed electronic digital computers and with the growing emphasis on numerical methods for engineering analysis. This method started as a generalization of the structural idea to some problems of elastic continuum problem, started in terms of different equations. Structural analysis is the most common application of finite element analysis. The term structural implies civil engineering structure such as bridge and building, but also naval, aeronautical and mechanical structure such as ship hulls, aircraft bodies and machine housing as well as mechanical components such as piston, machine parts and tools. The seven types of structural analyses in ANSYS and each of these analysis types are listed.

Static analysis

Modal analysis

Harmonic analysis

Transient dynamic analysis

Spectrum analysis

Buckling analysis

Explicit dynamic analysis

So from above structural analyses types, static structural analysis is used in this thesis. Static structural is used to determine the displacements, stresses, strains and forces in structures or components due to loads that do not induce significant inertia and damping effects. The kinds of loading that can be applied in a static analysis include externally applied forces and pressures, steady state inertial forces such as gravity or rotational velocity imposed (non-zero) displacements, temperatures (for thermal strain). A static analysis calculates the effects of steady loading conditions on a structure, while ignoring inertia and damping effects such as those caused by time varying loads. Static analysis can, however including steady inertia loads (such as gravity and rotational velocity), and time varying loads that can be approximated as static equivalent loads (such as static equivalent wind and seismic loads). Since we will analysis contact pressure and von misses stress for structural and thermal-structural analysis with ANSYS workbench. Here the methods for the analysis of finite element will be discussed.

4.1.2. Modelling of Disc and Pad Brake

The model made by using the CATIA software is converted into ‘igs’ then it is opened in the ANSYS workbench. The model consists of disc and two pads as shown below figure 4.1. Open ‘empty project’ and then click on the ‘Link to geometry file’ and then browse, select the required model in ‘igs’ format. Click on ‘new simulation’ option.

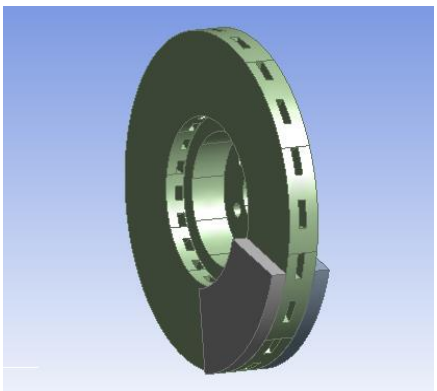

Figure 4.1: Assembly of Disc and Pads

4.1.3. Defining Material Properties of Study

The disc material is gray cast iron ISO standard with high carbon content with good thermo physical characteristics and the brake pad has an isotropic elastic behavior, whose thermo-mechanical characteristics adopted in this simulation in the contact pressure and von misses stress analysis of the two parts are recapitulated in Table 3.2 and Table 3.3. The required material properties are added into the software by using the tribo material properties. Then the next step is to enter the Young's Modulus and Poisson's ratio and density of the disc and pads material that have been used for analytical calculation in the previous chapter. This can be done by selecting the Engineering Data from the analysis tab of the ANSYS Workbench and inserting the corresponding values.

4.1.4. Defining Contact Region for Structural Analysis

Once the geometry is attached with Static Structural analysis tab, next thing is to define the contact between disc and pad. ANSYS has an inbuilt option, which automatically reads the attached geometry for any predefined contacts or other boundary definitions. The connection between the pad and disc is given as frictional contact, value of co-efficient of friction as 0.35 and it is provided in between the top face of the disc and bottom face of the pad. The figure below shows the contact being defined as frictional. One of the most important things is to change the Interface Treatment to " Adjust to touch". This option defines the kind of contact between the selected bodies. The figure below shows the image from ANSYS workbench showing the contact defined for disc and pad.

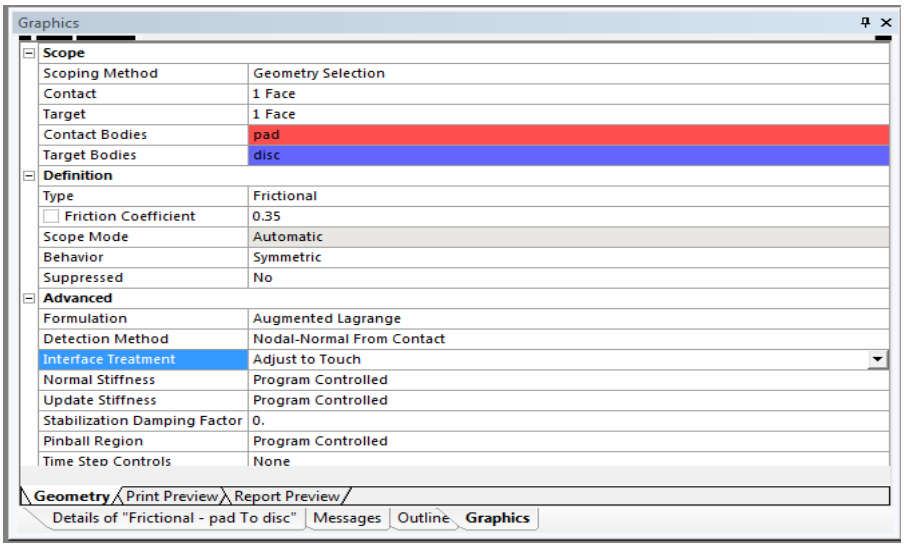

Figure 4.2: Image from ANSYS Workbench Showing Contact of Disc and Pad

4.1.5. Mesh Generation

The mesh with the default settings is not adequate to get the accurate results. In this analysis disc and pads were finely meshed with "Sizing" option in menu. The element size was chosen to be 0.0035 and also disc and pads contact surfaces were refinement. The image below shows the meshed assembly according to the given mesh size value. There are about 203792nodes and 107665elements to the entire geometries. The meshed view of the model is given in figure 4.3.

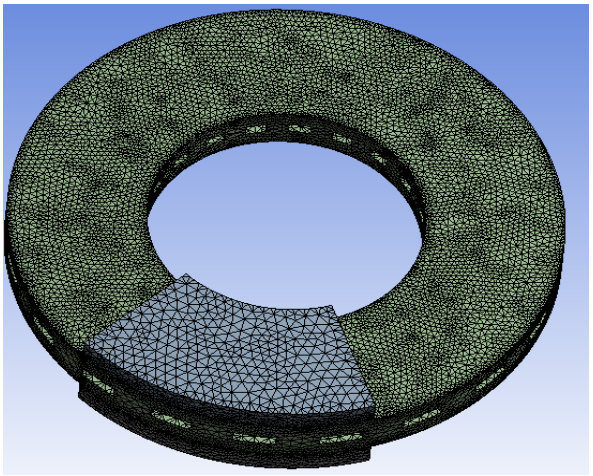

Figure 4.3: Meshed Model of Disc Brake with Pad

4.1.6. Boundary Conditions and Applied Loads to Structural Analysis

Here the displacement in the x and y direction of the outer round faces of the pads are arrested, so given the value as zero. At the same time, z direction displacement given as free, for allowing the movement of pads only in the z direction. Then displacement in the x and y direction of the outer and inner round faces of the disc made free. At the same time, z direction displacement is arrested, so given the value as zero, for allowing the movement of disc in the x and y direction. The variable pressure is applied in the top face of the pad. Along with that a rotational velocity of 91.77 rad/sec is provided for the hollow disc in the z direction, for the rotation of disc and this is clearly given in Figure 4.4.The selected data for the numerical analysis setting are summarized as follows:

- Total time of simulation =4.5sec
- Increment of time =1sec
- Number of load steps=1

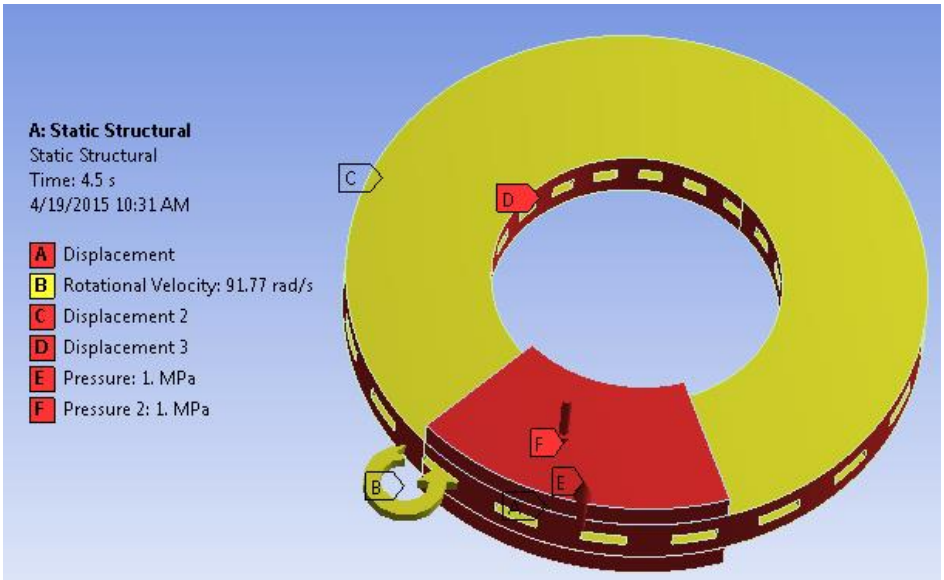

Figure 4.4: Boundary Conditions and Loads Statics Structural

4.2. Thermal-Structural Analysis

In the analysis of thermal-structural analysis of disc brake, the most important variables are pressure and temperature on the friction surface. So, we consider these applied loads in this thermal-structural analysis. The purpose of the analysis is to predict the contact pressure and corresponding von misses stress in the brake disc when the vehicle is subjected to sudden high speed stops as can occur under freeway driving conditions. In order to predict these values, the same material properties, structural boundary condition and applied loads, model were used as discussed above for static structural analysis. But some additional use full points to analysis these conditions were discuss as follow.

4.2.1. Defining Contact Region for Thermal-Structural Analysis

The geometry is attached with Thermal-Static Structural analysis tab, next thing is to define the contact between disc and pad. ANSYS has an inbuilt option, which automatically reads the attached geometry for any predefined contacts or other boundary definitions. The connection between the pad and disc is given as frictional contact, value of co-efficient of friction as 0.35 and it is provided in between the top face of the disc and bottom face of the pad. The figure below shows the contact being defined as frictional. One of the most important things is to change the Interface Treatment to "Adjust to touch". This option defines the kind of contact between the selected bodies. When meshing a model, the nodes on potential contacting surfaces comprise the layer of contact elements who's four Gauss integral points are used as contacting checkpoints.

The figure below shows the image from ANSYS Workbench showing the contact defined for disc and pad.

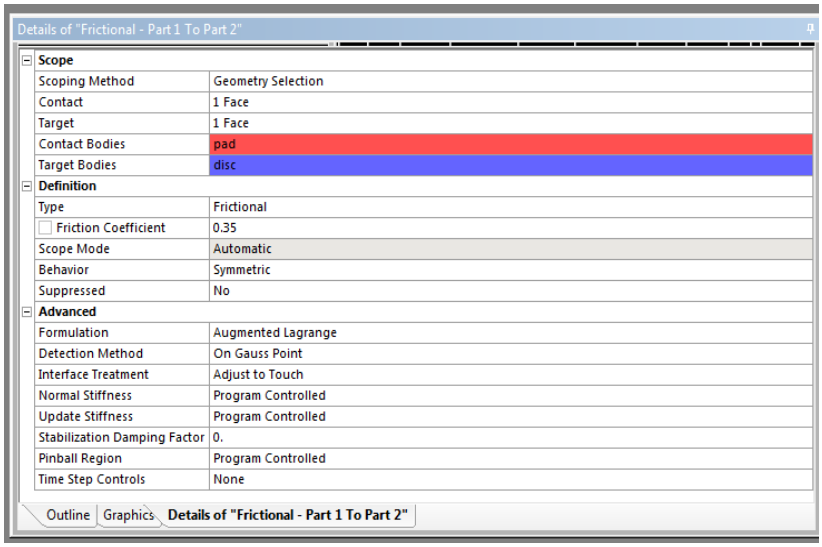

Figure 4.5: Image from ANSYS Workbench Showing Contact of Disc and Pad

4.2.2. Mesh Generation

Also mesh with the default settings is not adequate to get the accurate results. In this analysis disc and pad contact surfaces were refinement meshed with "Sizing" option in menu. The element size was chosen to be 0.001 and it was then refined at the contacting surfaces to get the finer mesh and continuous contact pressure and von misses stress values. The image below shows the meshed assembly according to the given mesh size value. There are about 352035 nodes and 223327 elements to the entire geometries. The meshed view of the model is given in the Figure 4.6.

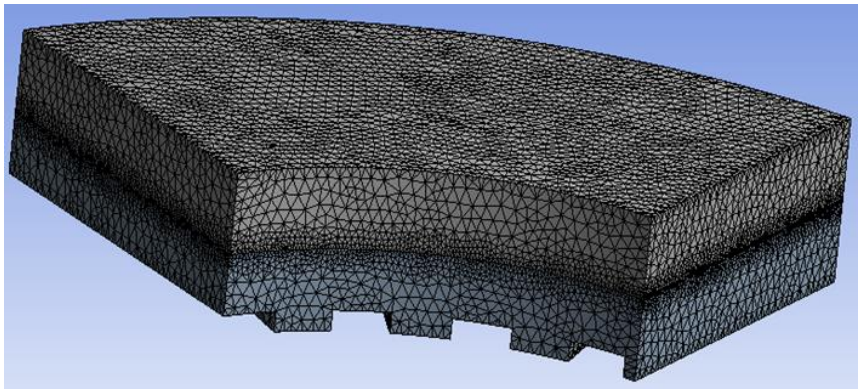

Figure 4.6: Meshed Assemblies Thermal-Structural

Boundary Conditions and Applied Loads to Thermal-Structural Analysis

By applying symmetric boundary condition, 1/8 th of the model is being simulated. Here the displacement in the x and y direction of the outer round faces of the pad is arrested, so given

the value as zero. At the same time, z direction displacement given as free, for allowing the movement of pad only in the z direction. Then displacement in the x and y direction of the outer round faces of the disc made free. At the same time, z direction displacement is arrested, so given the value as zero, for allowing the movement of disc in the x and y direction. The variable pressure is applied in the top face of the pad. The thermal loading is characterized by the thermal condition entering the disc and pad. The thermal calculation will be carried out by choosing the transient state and by introducing the physical properties of the materials. The selected data for the numerical analysis setting are summarized as follows:

- Total time of simulation =4.5sec
- Increment of time =1sec
- Number of load steps=1

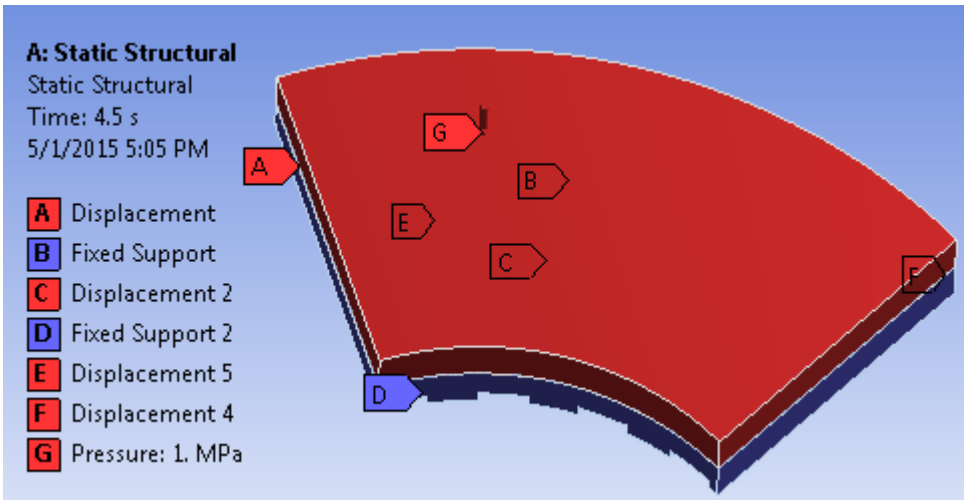

Figure 4.7: Boundary Conditions and Loads Thermal-Structural

Chapter Five

5. Results and Discussions

In this section, results of analytical method approach of contact temperature of disc brake, finite element approach for contact pressure and von misses stress without and within temperature effect estimation in ANSYS Workbench and analytical method is compared, analytical method approach of wear depth without and within temperature effect are discussed. Using both ANSYS Workbench software and analytical method, along with the boundary conditions, a variable brake pressure [MPa] is applied then we got a value for these aforementioned parameters. The result of the analysis summarized as follow.

5.1. Contact Temperature Variation of Disc Brake

Figure .5.1.Shows the contact temperature variation with time for different values of brake pressure at maximum contact temperature of disc brake. It is noticed that the contact temperature decreases with the increase of time. This is due to the convection through the air and the convection through the vanes of disc brake. The cooling increase significantly reduces the temperature gradient, in particular in the vicinity of the frictional surface. The graph is plotted using analytical analysis of contact temperature by Eq.3.56 and we have got an approximate graph to literature review [9].

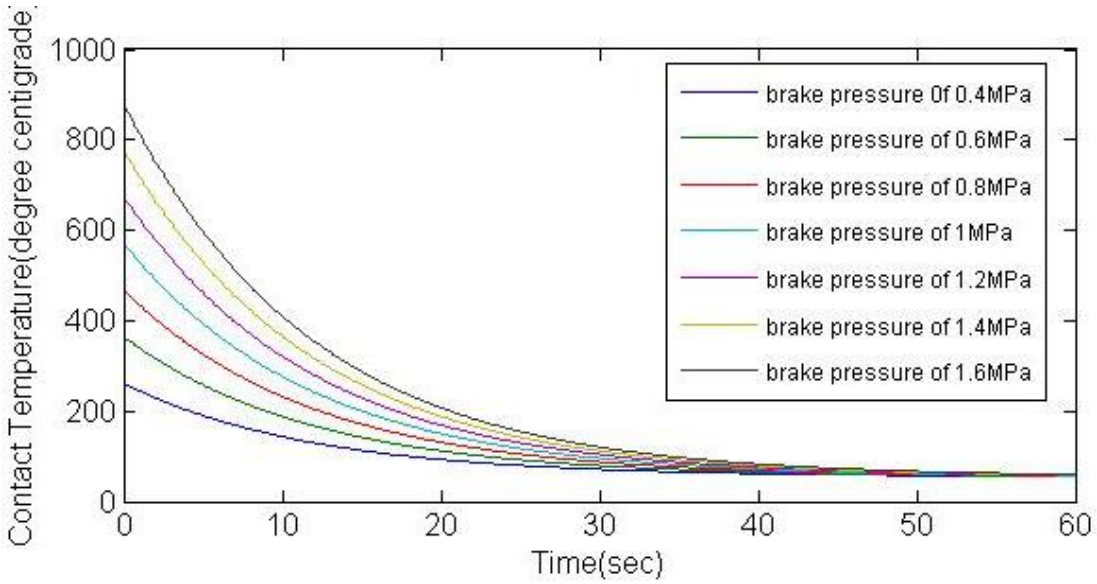

Figure 5.1: Variation of Contact Temperature at r=95.859mm with time (different Brake Pressure in MPa)

5.2. Contact Pressure Analysis by Structural Effect

Figure 5.2 shows that contact pressure distribution done by ANSYS workbench over disc brake during brake condition when applied brake pressure is 1MPa. As shown the contour plot maximum contact pressure is indicted by red color, which has a value of 3.134 MPa and its minimum value is 0 MPa also indicated by blue color. Also the figure depicted that the maximum contact pressure is high at outer and inner radius of disc brake.

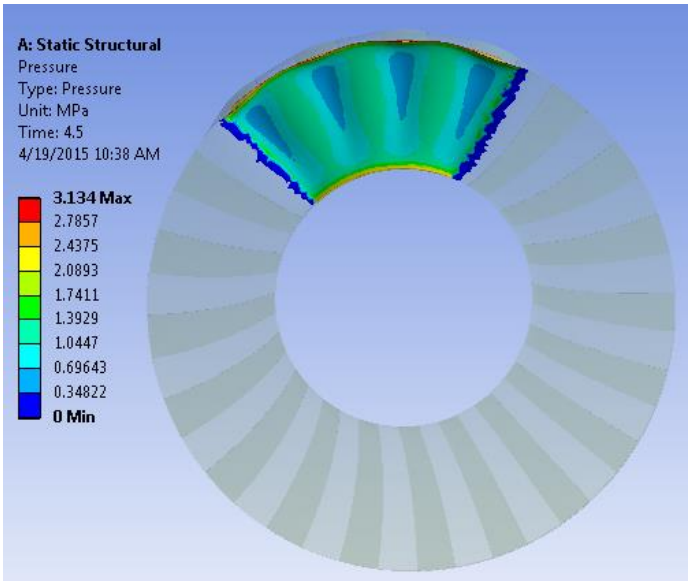

Figure 5.2: Contour Plot of Contact Pressure Distribution by Structural Effect

The same procedure used as Figure.5.2, and recorded maximum contact pressure with respect to each applied brake pressure in (MPa), is done by ANSYS workbench. And the analytical method is done by using Eq.3.7 with respect to each applied brake pressure in (MPa). And also maximum contact pressure the result is recorded in which done by it. The graph as shown in Figure 5.3, brake pressure with respect to contact pressure, is done by both methods. When we analyze the comparison between the analytical and ANSYS workbench software results, both the analytical and ANSYS workbench software results shows that the contact pressure increases with the increases of applied brake pressure. As shown in graph below, the maximum deviation is occurring at brake pressure of 0.4 MPa. At this brake pressure, the analytical result shows that the maximum contact pressure is 1.28 MPa. And the ANSYS workbench software result shows that the maximum contact pressure is 1.3257 MPa. The comparison of maximum contact pressure between the analytical and ANSYS workbench results is done and results have percentage error of 3.447%. So the comparison shows these values are in good agreement that the percentage error is less 10%. Also the

figure show the same result at 1MPa brake pressure for both analytical and ANSYS workbench. Most research papers were used this brake pressure to problems relate disc brake.

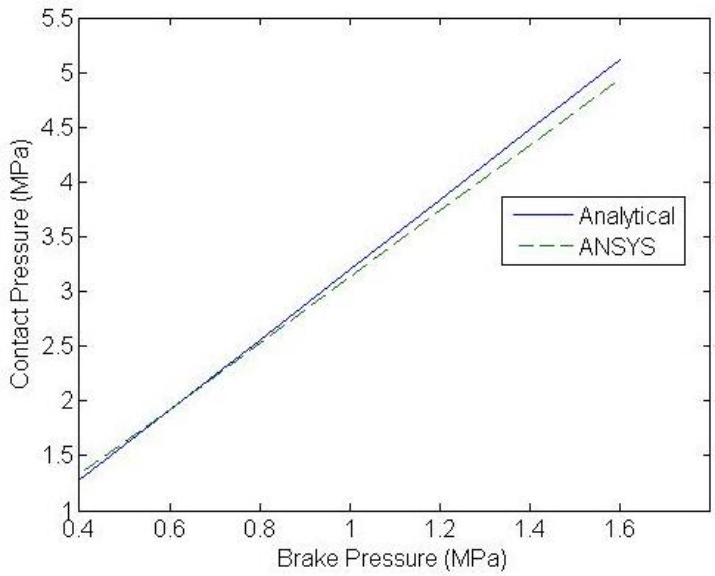

Figure 5.3: Brake Pressure with Respect to Contact Pressure Done by Methods.

5.3. Von Misses Stress Analysis by Structural Effect

Figure 5.4 shows von misses stress without temperature effect done by ANSYS workbench software over disc brake during brake condition when applied brake pressure is 1MPa. As shown the contour plot, von misses stress is indicating by red color, which has value of 6.597MPa and it minimum value is 869.82Pa also indicate by blue color. Also the figure depicted that the von misses stress is high at around peripheral edge of disc in contact with pad brake. . The bottom side figure below shows that magnified image of contact pressure on disc brake.

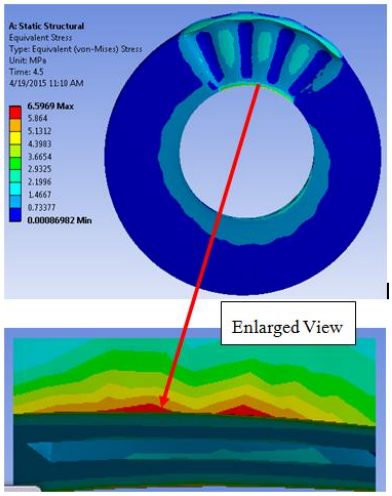

Figure 5.4: Contour Plot of Von Misses Stress Distribution without Temperature Effect

The same procedure used as Figure.5.2, and recorded von misses stress with respect to each applied brake pressure in (MPa), is done by ANSYS workbench. And the analytical method is done by using Eq.3.69 with respect to each applied brake pressure in (MPa). And also maximum von misses stress the result is recorded in which done by it. The graph as shown in Figure 5.5, brake pressure versus von misses stress which is done by both methods. When we analyze the comparison between the analytical and ANSYS workbench software results, both the analytical and ANSYS workbench software results shows that the von misses stress increases with the increase of applied brake pressure. As shown in graph below, the maximum deviation is occurring at brake pressure of 0.4 MPa. At this brake pressure, the analytical result shows that the maximum von misses stress is 2.526 MPa. And the ANSYS workbench software result shows that the maximum von misses stress is 2.766MPa. The comparison of maximum von misses stress between the analytical and ANSYS workbench results are done and results have percentage error of 8.68%. So the comparison shows these values are in good agreement that the percentage error is less than 10%. Also the figure show the 4.27% of error at 1MPa brake pressure for between analytical and ANSYS workbench. Most research papers were used this brake pressure to analyze problems relate disc brake.

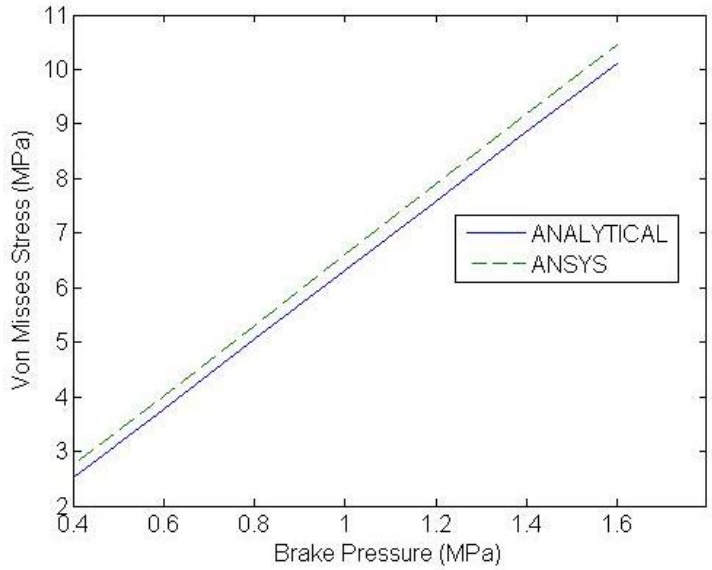

Figure 5.5: Comparison of Von Misses Stress for Structural Effect

5.4. Contact Pressure Analysis by Thermal-Structural Effects

Figure.5.6. shows contact pressure distribution done by ANSYS workbench software over disc brake during brake condition when applied both brake pressure is 1MPa, corresponding disc and pad temperatures are 571.3℃ and 2669.287℃ respectively. As shown the contour plot, maximum contact pressure is indicating by red color, which has value of 52.979MPa

and it minimum value is 0MPa also indicated by blue color. Also the figure depicted that the maximum contact pressure is high at near to midpoint of inner and center radius of disc brake and portions of vanes in contact with pad brake.

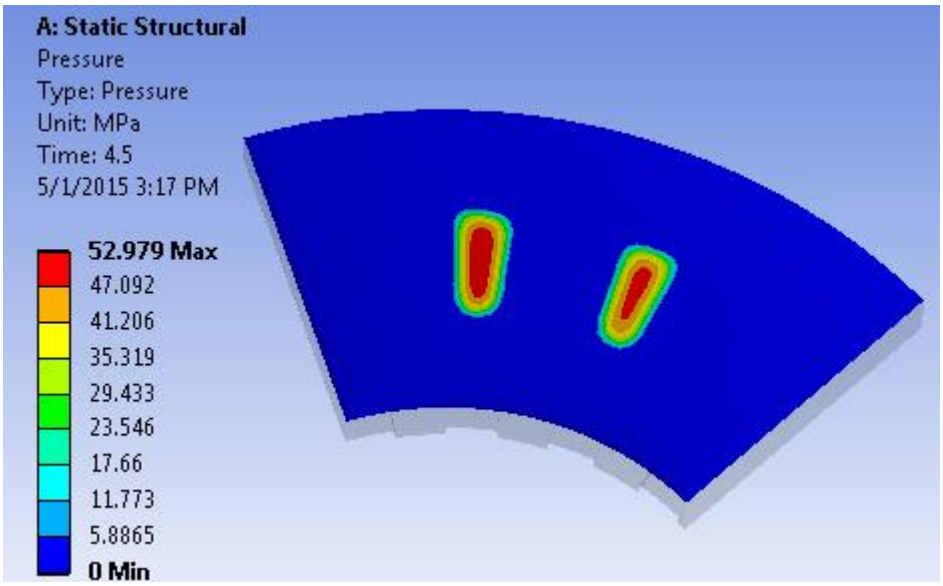

Figure 5.6: Contour Plot of Contact Pressure Distribution by Thermal-Structural Effects

The same procedure used as Figure.5.6, and recorded maximum contact pressure with respect to each applied brake pressure in (MPa) and contact temperature of disc and pad, are done by ANSYS workbench. And the analytical method is done by using Eq.3.63 with respect to each applied contact temperature of disc brake in (℃). And also maximum contact pressure the result is recorded in which done by it. The graph as shown in Figure 5.7, brake pressure with respect to contact pressure which are done by both methods. When we analyze the comparison between the analytical and ANSYS workbench software results, both the analytical and ANSYS workbench software results shows that the contact pressure increases with the increases of applied brake pressure. As shown in graph below, the maximum deviation is occurring at brake pressure of 0.4MPa. At this brake pressure, the analytical result shows that the maximum contact pressure is 22.4 MPa. And the ANSYS workbench software result shows that the maximum contact pressure is 21.044MPa. The comparison of maximum contact pressure between the analytical and ANSYS workbench results is done and results have percentage error of 6%. So the comparison shows these values are in good agreement that the percentage error is almost equal to 10%. Also the figure show the 5.39% of error at 1MPa brake pressure for between analytical and ANSYS workbench. Most research papers were used this brake pressure to analyze problems relate disc brake.

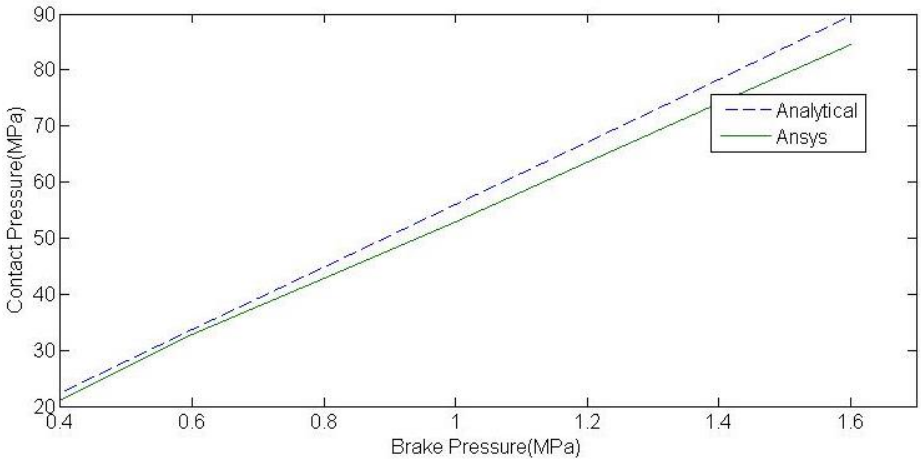

Figure 5.7: Comparison of Contact Pressure within Temperature Effect versus Brake Pressure

5.5. Von Misses stress Analysis by Thermal-Structural Effects

Figure.5.8. shows von misses stress with temperature effect done by ANSYS workbench software over disc brake during brake condition when applied both brake pressure is 1MPa, corresponding disc and pad temperatures are 571.3℃ and 2669.287℃ respectively. As shown the contour plot, maximum von misses stress is indicating by red color, which has value of 6.686GPa and it minimum value is 0GPa also indicated by blue color. Also the figure depicted that the maximum von misses stress is high at inner radius of disc in contact with pad brake. The bottom view figure show that magnified image of von misses stress at this point.

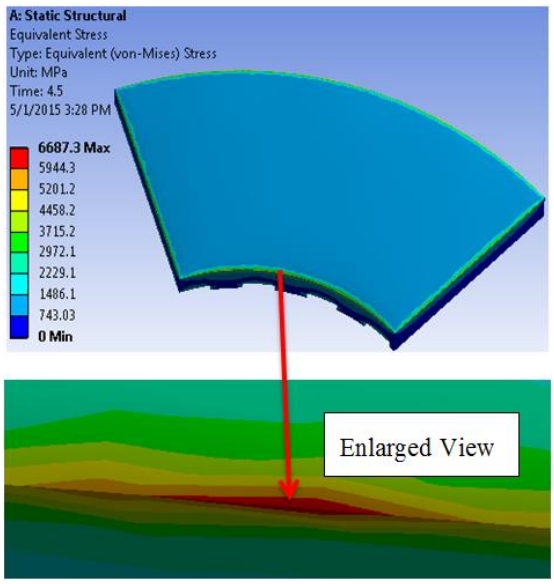

Figure 5.8: Contour Plot of Von Misses Stress Distribution within Temperature Effect

The same procedure used as Figure.5.8, and recorded maximum von misses stress with respect to each applied brake pressure in (MPa) and contact temperature of disc and pad, are

done by ANSYS workbench. And the analytical method is done by using Eq.3.72 with respect to each applied contact temperature of disc brake in (℃). And also maximum von misses result is recorded in which done by it. The graph as shown in Figure 5.9, brake pressure with respect to von misses stresses which are done by both methods. When we analyze the comparison between the analytical and ANSYS workbench software results, both the analytical and ANSYS workbench software results shows that the contact pressure increases with the increases of applied brake pressure. As shown in graph below, the maximum deviation is occurring at brake pressure of 0.4 MPa. At this brake pressure, the analytical result shows that the maximum von misses is 2.732GPa. And the ANSYS workbench software result shows that the maximum von misses is 2.916GPa. The comparison of maximum von misses stress between the analytical and ANSYS workbench results is done and results have percentage error of 6.3%. So, the comparison shows these values are in good agreement that the percentage error is less than 10%. Also the figure show the 2.11% of error at 1MPa brake pressure for between analytical and ANSYS workbench. Most research papers were used this brake pressure to analyze problems relate disc brake.

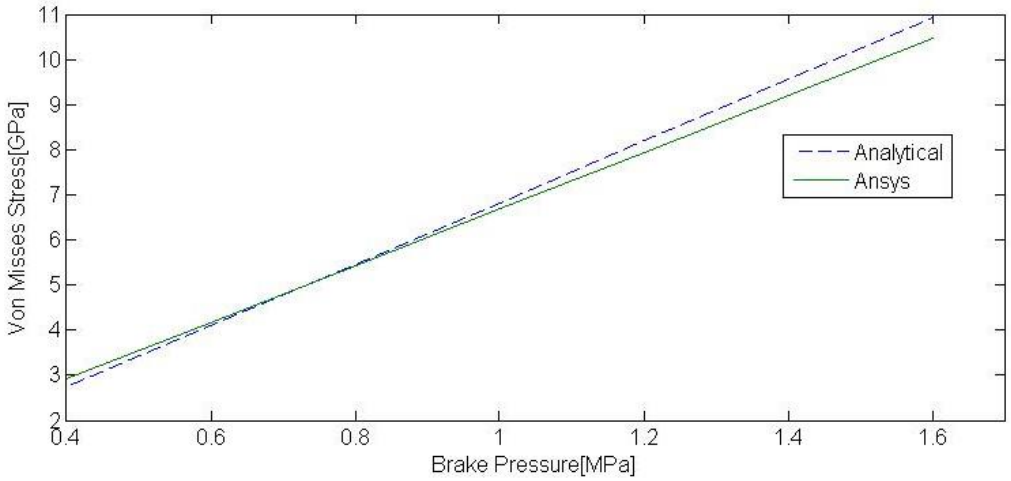

Figure 5.9: Comparison of Von Mise Stress within Temperature Effect versus Brake Pressure

5.6. Wear Depth Analysis by Structural Effect

The wear depth of disc brake without temperature effect is analysis both analytical method and ANSYS workbench from results of contact pressure. The analytical method of wear depth is analysis by using of Eq.3.11 with in different brake pressures. And it also analysis by ANSYS workbench by selection of maximum contact result from each applied brake pressure and then after we are use ARCHARD Eq.1.1. As shown Figure 5.10, when we are analysis the comparison between the analytical and ANSYS workbench software results, both

the analytical method and ANSYS workbench show that the wear depth increases with the increase of brake pressure.

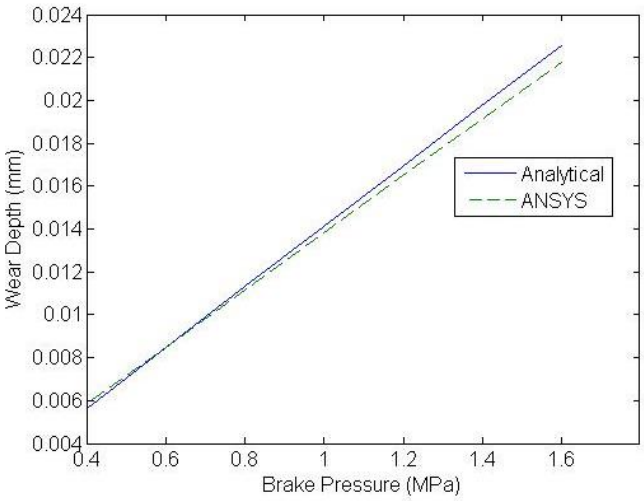

Figure 5.10: Comparison of Wear Depth without Temperature Effect versus Brake Pressure

5.7. Wear Depth Analysis by Thermal-Structural Effects

The wear depth of disc brake with temperature effect is also analysis both analytical method and ANSYS workbench results of maximum contact pressure with multiply by both velocity and wear coefficient. The analytical method of wear depth is analysis by using of Eq. 3.6 with in different brake pressures. And it also analysis by ANSYS workbench by selection of maximum contact pressure result from each applied brake pressure and disc brake temperature then after we are multiply it by both values of velocity at maximum contact pressure occur and wear coefficient. As shown Figure 5.11, when we are analysis the comparison between the analytical and ANSYS workbench software results, both the analytical method and ANSYS workbench show that the wear depth increases with the increase of brake pressure.

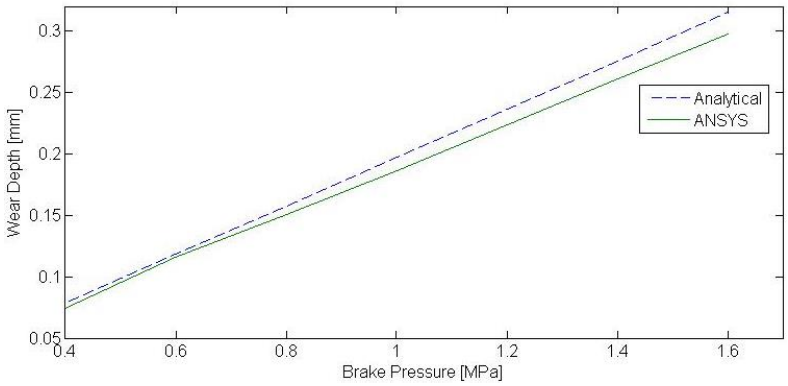

Figure 5.11: Comparison of Wear Depth Thermal-Structural versus Brake Pressure

Chapter Six

6. Conclusion and Future Work

6.1. Conclusion

In this thesis work is presented the analytical analysis and finite element method of surface wear on disc brake rotor without and within temperature effect. The method developed in this thesis work can be used to analysis contact pressure and wear in dry sliding contact for mechanical components. Comparison of ANSYS workbench result with analytical method is done and similar result is obtained with reasonable accuracy. So that, researchers may use both analytical and ANSYS workbench to predict contact pressure and wear of mechanical components related to with or without effect of temperature. Generally from this thesis work the following conclusions can be figure out.

- Analytical analysis of contact temperature distribution along radial direction of disc brake was estimated.
- The analytical analysis of contact pressure, wear depth and von misses stress estimated as function of brake pressure. The results from ANSYS workbench are approximate with analytical analysis.
- The critical point of contact for disc brake in contact with pad brake is identified in both analytical analysis and ANSYS workbench without or within temperature effects.
- When we compare, the effect of temperature in both methods of analysis results, without temperature effect is less than that of within temperature effect in all parameters (contact pressure, wear depth and von misses stress).
- There is a high contact pressure and von misses stress components at inner and outer radius of disc, and this may lead to failure of disc brake due to crack and fracture, because these parameters are as function of stress.

6.2. Future Work

In this thesis work contact pressure, wear depth and von misses stress are studied for different applied brake pressure of disc brake at dry condition without or within temperature effect. Other influence factors are not studied. So this work is restricted to specified cases. However, this paper can be extended to other situation listed below.

- The wear of disc brake within temperature effect would be interesting to conducted experimental study to validate the results of analytical analysis and ANSYS workbench software.
- The wear of disc brake under repeated braking condition within temperature effect should be conducted by both experimental and finite element method at specified applied brake pressure.
- The crack analysis for disc brake within temperature effect should be study at inner radius of the disc.

References

[1] Milenković, P.D., Jovanović, S.J., Janković, A.S., Milovanović, M.D., Vitošević, N.D., Đorđević, M.V., Raičević, M.M. (2010), "The Influence of Brake Pads Thermal Conductivity on Passenger Car Brake System Efficiency", Thermal Science, vol.14, pp.221–230.

[2] Akay, Adans (2002), "Acoustics of friction", Mechanical Engineering Department, Carnegie Mellon University, Pennsylvania.

[3] Ćirović, V. and Aleksendrić, D. (2011), "Dynamic modelling of disc brake contact phenomena", FME Transactions, Vol. 39, No. 1, pp. 177-183.

[4] Bayer, R. G. (1994), "Mechanical Wear Preditction and Prevention", New York.

[5] Hutchings, I. M. (1992), "Friction and Wear of Engineering Materials", CRC Press.

[6] Archard, J.F. (1953), "Contact and rubbing of flat surfaces", J. Appl. Phys., Vol. 24 No. 1, pp. 18-28.

[7] Kejela, T. (2014), "Thermal Stress Analysis of Disc Brake Rotor by Finite Element Method", AATT, AAU, Thesis.

[8] Talati, Faramarz (2009), "Analysis of Heat Conduction in a Disk Brake System", Spinger-Velag.

[9] Belchocine, Ali (2012), "Thermal Analysis of a Solid Brake Disc", Applied thermal engineering Vol. 32:59-67.

[10] Harpal, Singh (2012), "Thermal Analysis of Disk Brake using COMSOL", International journal on Engineering technologies ISSN No. 2249-3255.

[11] Sowjanya, K. (2013), "Structural Analysis of Disk Brake Rotor", International Journal of computer trends and technology- volume 4, Issue 7-July.

[12] Kuo, G.C. (2009), "Transient Temperature Analysis of a Cylindrical Heat Equation", Department of Mechanical Engineering, Nanya Institute of Technology, July.

[13] Shah, Q.H. (2011), "Surface Temperature Distribution in a Composite Brake Rotor", Department of Mechanical Engineering ,International Islamic University Malaysia.

[14] Belhocine, Ali (2014), "Structural and Contact Analysis of Disc Brake Assembly During Single Stop Brake event", Faculty of Mechanical Engineering, University of Sciences and the Technology of Oran, Algeria.

[15] Tirovic, M. and G. Ali (2001), "Design Synthesis of non-Symmetrically Loaded High-Performance Disc Brakes: Part 1**",** Vol. 215, pp. 101-109.

[16] Imam, syafa'at (2012), "Prediction of Sliding Wear of Artificial Rough Surfaces", Department of Chemical Engineering Diponegoro University, Semarang Indonesia, September 12-13.

[17] Alen, John (2014), "Stress Analysis of Polyoxymethylene which Leads to Wear in Pin on Disc Configuration using Finite Element Method", Department of Mechanical Engineering, India International Journal of Research in Advent Technology, Vol.2, No.4, April E-ISSN: 2321-9637.

[18] Molinari, J.F. (2000), "Finite-element modeling of dry sliding wear in metals", California *Institute of Technology, Pasadena, California,* USA.

[19] Podra, P., Andersson, S. (1999), "Simulating Sliding Wear with Finite Element Method", Tribology International, 32:71-81.

[20] Hairier**,** J. B.(1955), "Themie Analyaque de la Chaleur", Paris, 1822 (English .trans. by A. Freeman, Dover Publications, Ncw York, 1955).

[21] Belhocine, A. and Bouchetara, M. (2012), "Simulation of Fully Coupled Thermo-Mechanical Analysis of Disc Brake Rotor", University of of Oran WSEAS transactions on applied and theoretical mechanics Issue 3, Volume 7.

[22] Majcherczak, D., Dufrenoy, P. and Berthier, Y. (2007), "Tribological, Thermal and Mechanical Coupling Aspects of the Dry Sliding Contact", Tribol Int 40:834–843. doi: 10.1016/j.triboint.2006.08.004.

[23] Khalid, M.K., Mansor, M.R., Abdul Kudus, S.I., Tahir, M. M., Hassan, M. Z. (2011), "Performance Investigation of the UTeM Eco- Car Disc Brake System", International Journal of Engineering and Technology, Vol. 11, No. 6, pp. 1-6.

[24] Limpert, R. (1999), "Brake Design and Safety", 2nd Edition, Warrendale, Pennsylvania, Society of Automotive Engineering Inc., pp. 137-144.

[25] Hertz, H. (1881), "On the contact of elastic solids", J. reine angew. Math, 92(156-171):110.

[26] Hills, D. A. and Nowell, D. (1994). Mechanics of fretting fatigue. Solid mechanics and its applications vol. 30. Kluwer Academic Publishers.

[27] Johnson, K. L. and Johnson, K. K. L. (1987), "Contact mechanics", Cambridge University press.

[28] Midlin, R. D. and Deresiewicz, H. (1953), "Elastic Spheres in Contact Under Varying Oblique Forces", ASME Journal of Applied Mechanics, vol. 20 (3), p. 324-344.

[29] Timoshenko, S.P. and Goodier, J.N. (1951), "Theory of Elasticity", McGraw-Hill, New York.

[30] Oder, G., Reibenschuh, M., Lerher, T., Šraml, M., Šamec, B., Potrč,I. (2009), "Thermal and Stress Analysis of Brake Discs in Railway Vehicles", Advanced Engineering 31, ISSN 1846-5900.

[31] Nega, T. (2014), "Finite Element Based Surface Wear Analysis of Cam and Follower System", AAU, Thesis, pp.39-42.

[32] Jang, H., Ko, K., Kim, S. J., Basch, R. H. and Fash, J. W. (2004), "The Effect of Metal Fibers on the Friction Performance of Automotive Brake Friction Materials", Wear, 256, pp. 406-414.

[33] Ling, F. F. (1973), "Surface mechanics", John Wiley & Sons, New York.

[34] Blok, H. (1940), "Fundamental Mechanical Aspects in Boundary Lubrication", SAE Trans., Vol. 46, 54-68.

[35] Nowacki, W. (1962), "Thermo-elasticity", Pergamon Press, Oxford.

[36] Kreith, F. (1965), "Principles of Heat Transfer, International", Textbook Company, Scranton, Pennsylvania.

[37] Limpert, R. (1975), "Cooling Analysis of Disc Brake Rotors", SAE Paper No. 751014, Truck Meeting, Philadelphia.

[38] Limpert, R. (1992), "Brake Design and Safety", Second ed. Warrendale, Science of Automotive Engineers Inc., USA.

[39] Tian, X. and Kennedy, F. E. (1994), "Maximum and Average Flash Temperature in Sliding Contacts", ASME J. Tribol., vol. 116, pp. 167-173.

[40] Barber, J.R. (1975), "Thermo-elastic Contact of a Rotating Sphere and a Half-Space", University Department of Mechanical Engineering, Newcastle upon type, Gt. Britain.

[41] Thomas.J.Mackin,"Thermal cracking in disc brakes", Department of mechanical and industrial engineering, The University of Illinois at Urbana-Champaign, 2000.

[42] Keith Nisbett, J.(2009), "Shigley's Mechanical Engineering Design", eighth edition.

[43] Budynas, Richard G. (Richard Gordon), " Shigley's mechanical engineering design ",Richard G. Budynas, J. Keith Nisbett. —9th ed.

[44] Benabdallah, H. and Olender, D. (2006), "Finite Element Simulation of the Wear of Polyoxymethylene in Pin-On-Disk Configuration", Wear 261, 1213-1224.

[45] Hegadekatte, V., Huber, N. and Kraft O. (2005), "Finite Element Based Simulation of Dry Sliding Wear", Modelling Simul. Mater. Sci Eng., VOL.13:57-75.

[46] Podra, P. and Andersson, S. (1999), "Simulating Sliding Wear with Finite Element Method", Tribology International 32, 71-81.

[47] ANSYS User Manual, Version 14.5, online documentation

Appendix I: Specification SUV Car

	- Manual operated - 4 WD and 2 WD -Gear-ratio- I:4.016;II:2.318;III:1.401;IV:1.000;V:0.778;R:3.549
Steering mechanism	- Model - ZDZ7 - Circulating ball power steering, hydraulic assisted
Rack	- Front over suspension - Dual cross member independent, torsion bar - Rear cover suspension - torsion bar,5 bar coil spring
Wheel	- Rim - Aluminum type,17 inch - Tire -235/75R Spare tire
Cab	- Type - all metal closed with AC - Seats - 5 seats - electronic type AC and DVD entertainment system with Bluetooth - Door - has indicator light has remote control - Seat cloth - leather laminated - Remote control of rear view mirror - Motor operated window glass - Electrical control of side indicator light under rear view mirror
Frame	- Mitsubishi tech.
Wheel Alignment	- Camber angle - 10’-10 10’ - Caster angle - 20 - 40 * The gap should be in – out (3 – 5) (mm)

Others	- Car model - DD6470C - Color - lver/black - Safety energy absorbing steering column -Air bag
Breaking	- Parking brake - Handle cable, central control,Drum type - Front brake - Disc type - Rear brake - Disc type -Brake type-ABS+EBD -Hydraulic pressure 1Mpa -81m stopping distance -Emergency braking time 4.5sec.
Over all weight	-Only vehicle (kg)-1860 -Vehicle and load and also passenger + deriver (2510)